Yao *et al.*
Progress in Earth and Planetary Science (2024) 11:31
https://doi.org/10.1186/s40645-024-00636-9

Progress in Earth and Planetary Science

RESEARCH ARTICLE

Open Access

Fluvial geomorphic parameters of the Shuiluo River Catchment and their tectonic implications, SE Tibetan Plateau

Wei Yao[1], Xiaoxi Lyu[1*], Dongning Lei[2,3*] and Peng Wu[4]

Abstract

The Shuiluo River Catchment (SRC) is the front zone of the southeast compression and uplift of the Tibetan Plateau, with intense tectonic activity. In the basin, a series of regional large NW–SE trending active faults are developed. Studying clearly the geomorphic evolution of the SRC is conducive to further understanding the uplift and expansion mechanism of the SE edge of Tibetan Plateau. Our research was based on geographic information system, numerical analysis tool, and digital elevation model data, to extract six geomorpic parameters (*hypsometric integral*, *asymmetry factor*, *basin shape ratio*, *valley floor width–valley height ratio*, *normalized channel steepness index* and *index of relative active tectonics*) in SRC. After eliminating the impacts of climate, catchments area, and glacier, the geomorphic evolution of the SRC is mainly affected by geological structure and differential tectonic uplift movement; in the upstream and midstream (upper part), the shape of valleys and stream longitudinal profile shapes are affected by lithology; affected by geological structure and tectonic uplift, the tectonic activity in the midstream and downstream is relatively strong, and the intensity of activity in the downstream is stronger than that in the midstream, which may suggest that the faults' activity in the downstream is stronger; *the index of relative active tectonics* values of the SRC are consistent with the regional seismic intensity, field-work and low-temperature thermochronology which indicates it is reasonable to use the fluvial geomorphic parameters to study the regional geomorphic evolution. The morphological parameters we extracted show different values in different regions of SRC, which may be the result of differential uplift in the southeastern of the Tibetan Plateau.

Keywords SE Tibetan Plateau, Shuiluo River Catchment, Tectonic activity, Fluvial geomorphic parameters

*Correspondence:
Xiaoxi Lyu
karstlv@gznu.edu.cn
Dongning Lei
lei_dongning@163.com
[1] School of Karst Science, Guizhou Normal University, Guiyang 550001, China
[2] Key Laboratory of Earthquake Geodesy, Institute of Seismology, China Earthquake Administration, Wuhan 430071, China
[3] Wuhan Institute of Earthquake Engineering Co., Ltd., Wuhan 430071, China
[4] College of Geographic Science, Harbin Normal University, Harbin 150025, China

1 Introduction

Since the Cenozoic, along with the collision of the Indian and Eurasian plates, and resulting compression, the highest in the world has been formed-Tibetan Plateau (Molnar and Tapponnier 1975; England 1997; Chen et al. 2017; He et al. 2023; Ma et al. 2023a, b). The Tibetan Plateau has a profound impact on atmospheric circulation and thus global climate, and is an ideal place for scientific research (Tapponnier 2001). Due to the uplift effect of the Tibetan Plateau, as well as the mutual compression of multiple sturdy and almost undeformed cratons such as the Tarim, North China Craton, and South China Block on its eastern and northeastern edges, some orogenic belts have been formed, resulting in the thickening of the crust around the plateau and the uplift of blocks that is still ongoing (Tapponnier and Molnar 1977; Ding et al. 2022; Sun et al. 2023). Regional fault zones are widely developed around the Tibetan Plateau, such as Xianshuihe-Xiaojiang fault, Altun fault, Kunlun fault, and Yushu fault (Chen et al. 2016; Ji et al. 2020; Tian et al. 2021). These large faults are generally the result of strong tectonic activity (He et al. 2010; Li et al. 2021). Simultaneously triggering strong earthquakes, landslides and mudslides (Chen et al. 2023; Huang et al. 2023). The study of these fault zones can reveal the tectonic activity and orogenic belt information in the periphery of the Tibetan Plateau, and then we can further analyze the uplift mechanism of the plateau (Li et al. 2016; Wu et al. 2023a, b). These fault and orogenic belts have been studied by many scholars (Wang et al. 2008, 2014; Li et al. 2015, 2021; Yan et al. 2017; Chen et al. 2020; Yin and Luo 2021; Tian et al. 2023; Shi et al. 2023; Luo et al. 2023), which further enriched the research base of the Tibetan Plateau. Understanding the activity mechanisms and differential activity of these active faults is beneficial for understanding the characteristics of the Cenozoic tectonic landforms around the Tibetan Plateau and even the tectonic movements of the entire it and theirs tectonically implications.

In addition to the active fault and orogenic zone, the river, as a unique geomorphic unit, is also extremely sensitive to the response of tectonic activities. River morphology reflects tectonic activity and, in particular, river long profiles reflect uplift histories (Wang et al. 2021). The fluvial geomorphologic features, such as the terrace deposits on both sides of the river, and the shape of the horizontal and vertical sections of the river, can reflect rich information of tectonic activities (Ma et al. 2023a, b). Fluvial geomorphology has become the most ideal carrier for recording tectonic activities (Howard and Kerby 1983; Burbank et al. 1996; Snyder et al. 2000; Clark and Handy Royden 2000). Many studies use fluvial geomorphology to reveal regional differential tectonic activities, tectonic geomorphologic features, and geological age (Partabian et al. 2016; Ahmad et al. 2018; Anand and Pradhan 2019; Wang et al. 2022). Some geomorphic parameters such as mountain front sinuosity (SMF) (Amine et al. 2020), fractal dimension (FD), normalized channel steepness index (k_{sn}) (Whipple and Tucker 1999), valley floor width–valley height ratio (VF) (Cannon 1976; Bull and Mcfadden 1977), and hypsometric integral (HI) (Strahler 1952), which can be used to quantitatively explore the characteristics of regional fluvial geomorphology, especially in some areas lacking ideal dating materials (Aier et al. 2011; Lahiri and Sinha 2014; Amine et al. 2020; Buczek and Górnik 2020; Ali et al. 2021; Wang et al. 2021; Yu et al. 2022). Because the rivers are very sensitive to the tectonic uplift at the edge of the Tibetan Plateau, the use of fluvial geomorphology to study neotectonics has become the main direction of the academic community, and then many researches have been carried out (Su et al. 2016; Fan et al. 2018; Luo et al. 2023). The study of the tectonic evolution history around the Tibetan Plateau focuses on its northeast and southeast edges (Chang et al. 2015; Chen et al. 2018; Gao et al. 2019; Sun et al. 2022; Wang et al. 2022; Zhou et al. 2023a, 2023b; Tan et al. 2023; Wu et al. 2023a, b). Compared with the northeastern edge of the plateau, which is widely used for dating techniques in the Quaternary system, there is relatively limited research on the chronology of eroded bedrock landforms in the southeastern edge, mainly characterized by high mountains and canyons, especially in some typical active tectonic basins (Williams 1987; Zhou et al. 2005; Chang et al. 2015). Located at the SE of Tibetan Plateau and in the southern part of the Songpan-Ganzi fold belt, the Shuiluo River Catchment (SRC) is a large-scale basin (catchment area >10,000km^2) in the southern part of the western Sichuan Plateau, and it is a primary tributary of the midstream of the Jinsha River; on the meanwhile, the catchment is in the transition area from the Zhongzan block to the Erlong block and the Yangtze paraplatform (Nie et al. 2015). And it is surrounded by the Ganzi Litang fault, Jinshajiang fault, Yulongxueshan fault and Lijiang fault, and some faults of northwest and northeast trend are also developed in the region, the regional tectonic condition is extremely complex. Previous studies on the tectonic evolution history of the region around the SRC (SE edge of the Tibetan Plateau) have shown that there are significant spatial differences in the rate of tectonic denudation and uplift time in southeastern Tibetan Plateau (Zhang et al. 2017). The response of the SRC to these differential tectonic activities is an important area for understanding

the geomorphic evolution of southeastern Tibetan Plateau, and the dense river network developed on the surface of the SRC provides a research window. Therefore, the study of the fluvial geomorphology in the basin is conducive to interpret the characteristics of regional tectonic activities. Moreover, the evolution of the ancient Shuiluo River (~1.7 Ma) stream network system is the key to unlocking the formation and evolution mechanism of the first bend of the Yangtze River (Kong et al. 2012; Zhang et al. 2022). Therefore, a systematic study of the river geomorphic evolution of Shuiluo River is conducive to further clarifying the compression and uplift mechanism of the southeastern edge of the Tibetan Plateau, as well as related scientific issues related to the formation and evolution of the first bend of the Yangtze River. The digital elevation model (DEM) is an important tool in quantitative study of geomorphic evolution, which is widely used in the research of digital geomorphology because it is easily accessible (Chang et al. 2015; Tang et al. 2017; Xiong et al. 2021).

In order to use fluvial geomorphic parameters to explain the differences of SRC tectonic activity and reveal its response to the uplift of the Tibetan Plateau, we extracted six geomorphic parameters of the SRC through geographic information system (GIS) and numerical analysis tool based on DEM data in this work: *hypsometric integral (HI)*, *asymmetric factor (AF)*, *shape basin ratio* (*BS*), *valley floor width–valley height ratio* (*VF*) and *Normalized Channel Steepness Index* (k_{sn}). We analyzed the fluvial geomorphic features of the studied basin by above-mentioned six geomorphic parameters and calculated the *Index of Relative Active Tectonics* (*RIAT*) of the SRC by the method of tectonic activity classification (Hamdouni et al. 2008). Combined with regional geological data, glacier distribution, earthquake, precipitation data and field work, we analyzed the main factors affecting the fluvial geomorphic evolution of the SRC, and then discuss the relative differences in tectonic activity in the study area and their response to the compression and uplift mechanisms of the SE Tibetan Plateau margin. In order to clearly show the spatial differences in the activity tectonic of SRC based on our work results, and for ease of expression, we define the area from the catchment source to Maiwa as the upstream section of SRC, that is, the north, and the area (or river section) between Maiwa and Shuiluo as the midstream (that is, the center). The following areas are defined as downstream, i.e., southern (Fig. 2).

2 Study area

2.1 Fluvial network features

The Shuiluo River originates from the west side of Donglang mountain in the north of Daocheng, Sichuan Province, and flows southwestward through Sangdui and Maiwa, then flows southward through Mairui and Shuiluo, then flows southward through the southwest of Litang, and finally flows into the Jinshajiang River at the Sanjiangkou at the border of Ninglang, Yunnan Province, which is a primary tributary of the left bank of the midstream of the Jinsha River (Fig. 1a–c). The latitude is 99.87–100.81°E, 27.62–29.57°N and the basin area is about 13,825 km^2. we used the hydrology tool of ArcGIS 10.2 to obtain the drainage basin network and catchment range of SRC, and to divide its 41 sub-catchments. We finally determined the spatial position of the main stream channels (primary tributary) of SRC and of 41 sub-catchments. The area of the sub-catchment on the left bank of the mainstream is small, only No.3 sub-basin has a large area about 1,310km^2 and the other sub-basins have small area. On the right bank, there are large sub-basins namely Nos. 22, 37 and 38, with an area of 1789 km^2, 2978 km^2 and 1186 km^2, respectively. The mainstream of Shuiluohe River is about 299km long, and shorter rivers are developed along the east bank of the mainstream, with an average length of 16.94 km (Fig. 2, Table 1). The elevation drop of the basin is 4009 m, and the elevation of the northern part of the basin is high, followed by the central part. The elevation of sub-basins 38, 40 and 41 in the south is the lowest, with an altitude range of 2312–3423 m (Fig. 2).

2.2 Geomorphology and geology

The swath topography profile shows that the valley in the midstream and downstream (central and southern parts, A-A'; B-B') of SRC is extremely deep, and the peaks are even steeper. In the midstream, there are also three snow capped mountains with an altitude of over 5000 meters, including Yangmaiyong, XhanuoDuoji, and Senaichi in Daocheng Yading Scenic Area. There are many faults distributed in this region. This region stratum mainly consisting of Triassic limestone, sandstone, slate, etc. Upstream of SRC (north, C-C'), there are larger and higher altitude plateau surface developed, with fewer faults and more granite distributed. Quaternary sediments are developed in the central valley from Sangdui to Maiwa in upstream of SRC (Figs. 1c, 3). The strata and lithology of the SRC are complex, with strata exposed from Proterozoic to Cenozoic, mainly composed of marine Triassic limestone and metasandstone. In the northern part of the basin, Triassic porphyry monzogranite is distributed; the eastern part is dominated by limestone, sandstone and slate of the upper Triassic Yidundaochengqugasi Formation of the basin facies; the southern part is dominated by basalt with slate and tuffaceous rock; the southwestern part is dominated by slate with basalt and thin limestone of the lower and middle

Triassic Niru Formation of the basin facies; the southeast is dominated by basaltic breccia of the Middle and Upper Permian Zhongdagai Formation (Figs. 1c, 3). The SRC is surrounded by Jinshajiang Fault, Yulongxueshan Fault, Ganzi-Litang Fault and Lijiang Fault. Ganzi-Litang Fault is about 600 km long, which is the boundary of Yidun and Songpan-Ganzi blocks, and its northwest end is connected with Jinshajiang Fault (Jackson et al. 2020). According to field structural observation, rock mass age and chemical characteristics, it is shown that Ganzi-Litang Fault and Jinshajiang Fault are continuous structural elements across the eastern Tibetan Plateau (Reid et al. 2007). The southeast end of Ganzi-Litang Fault is located in the transitional zone between the Yangtze paraplatform and the Qiangtang block (Burchfiel et al. 1995). The Ganzi-Litang Fault is one of the most important active fracture zones on the Western Sichuan Plateau and is also a major trigger of intense tectonic activity on the plateau (Zhang et al. 2017). The Jinshajiang Fault entered Yunnan from Derong, Sichuan, and went south along the valley of the middle section of the Jinshajiang River. This fault is a large strike slip fault that controls the southwest edge of the Kangdian block (Duan and Tan 2000). The activity of the middle section of Jinshajiang Fault is stronger than that of the north section, and the activity of the north section is weaker since the late Pleistocene (Chang et al. 2019). Lijiang Fault is the SW-trend extension of the Mesozoic Longmenshan-Jinpinshan thrust nappe structural belt, and it is located in a strong erosion and deep cutting area, lacking Quaternary sediments. Since the Holocene, three ancient earthquakes in Lijiang-Xiaojinhe Fault caused the complete rupture of the middle section of the fault, resulting in the development of the structural fracture zone in this section (Ding et al. 2018). In the studied catchment, a series of NW and NE faults are also developed.

3 Overview of DEM data and methodology

Our research was based on the global high-resolution DEM data (https://www.earthdata.nasa.gov/esds/competitive-programs/measures/nasadem) released by National Aeronautics and Space Administration (NASA) on February 18, 2020, after reprocessing Shuttle Radar Topography Mission (SRTM) data, which improves the elevation accuracy and fills the missing values. The spatial resolution of DEM data is 30m, covering from 60 ° N to 56° S. The spatial reference of DEM data we used is World Geodetic System (WGS) 1984, and we used geographic information system (GIS) to cut and project the DEM data (WGS 1984 Universal Transverse Mercator Zone 47N). Then we used the hydrology tool of ArcGIS 10.2 software provided by Environmental Systems Research Institute (ESRI) to obtain the drainage basin network and basin range of SRC, and to divide its 41 sub-catchments. Finally determined the spatial position of the main stream channels of SRC and of 41 sub-catchments. We used GIS, CaIHypso (an ArcGIS extension tool for calculating hypsometric integral curves) and MATLAB (a mathematical software produced by MathWorks in the USA), combined with parameter model, to obtained six geomorphic parameters.

3.1 Hypsometric Integral (HI)

Hypsometric integral (HI) is a mathematical model that reflects the relationship between the development stages of catchment geomorphology and erosion. It displays the period (stage) of geomorphic development. Hypsometric curves display the stages of geomorphic evolution. When the curve is convex, it indicates that there is more material to be eroded on the surface, and the topography on the surface is undulating greatly, which represents an early stage of geomorphic evolution. When the curve shows a concave shape, it represents the late stage of topography development, where the amount of eroded material on the surface increases and the surface relief decreases. The *HI* value directly reflects the stage of geomorphic development. $HI < 0.40$, the geomorphic evolution reaches the maturity stage, and the intensity of tectonic activity is not strong; $0.40 \leq HI < 0.50$, the geomorphic evolution reaches the middle stage, and the tectonic activity is relatively strong; when $HI \geq 0.50$, the geomorphic evolution reaches early stage, and has extremely strong tectonic activity (Strahler 1952). *HI* was proposed by Strahler, and the calculation formula is:

$$HI = \frac{h_{mean} - h_{\min}}{h_{\max} - h_{\min}} \quad (1)$$

(See figure on next page.)

Fig. 1 Location, lithology and geological structure of SRC. **a** Location of the Tibetan Plateau in the world, **b** main faults and tectonic divisions developed in the Tibetan Plateau, and the SRC is located in the southeast of the Tibetan Plateau, **c** tectonic diagram of study area. Lithology and faults data are from https://geocloud.cgs.gov.cn/, and the resolution is 1:500000. F1. Zhongdian-Xiangcheng Fault. F2. Xisashi Fault. F3. Lide-Dewu Fault. F4. Shade Fault. F5. Hehaizi Fault. F6. Sanyanlong Fault F7. Mengzi Fault. F8. Chitu Fault. F9. Boke Fault. F10. Qiasi Fault. F11. Ranglang Fault. F12. Guaishaoti Fault. F13. Lagengwa Fault. F14. Yangta Fault. F15. Zhangke Fault. F16. Jinpingshan Fault. F17. Longpan Fault. Note: the swath topography profile see Fig. 3

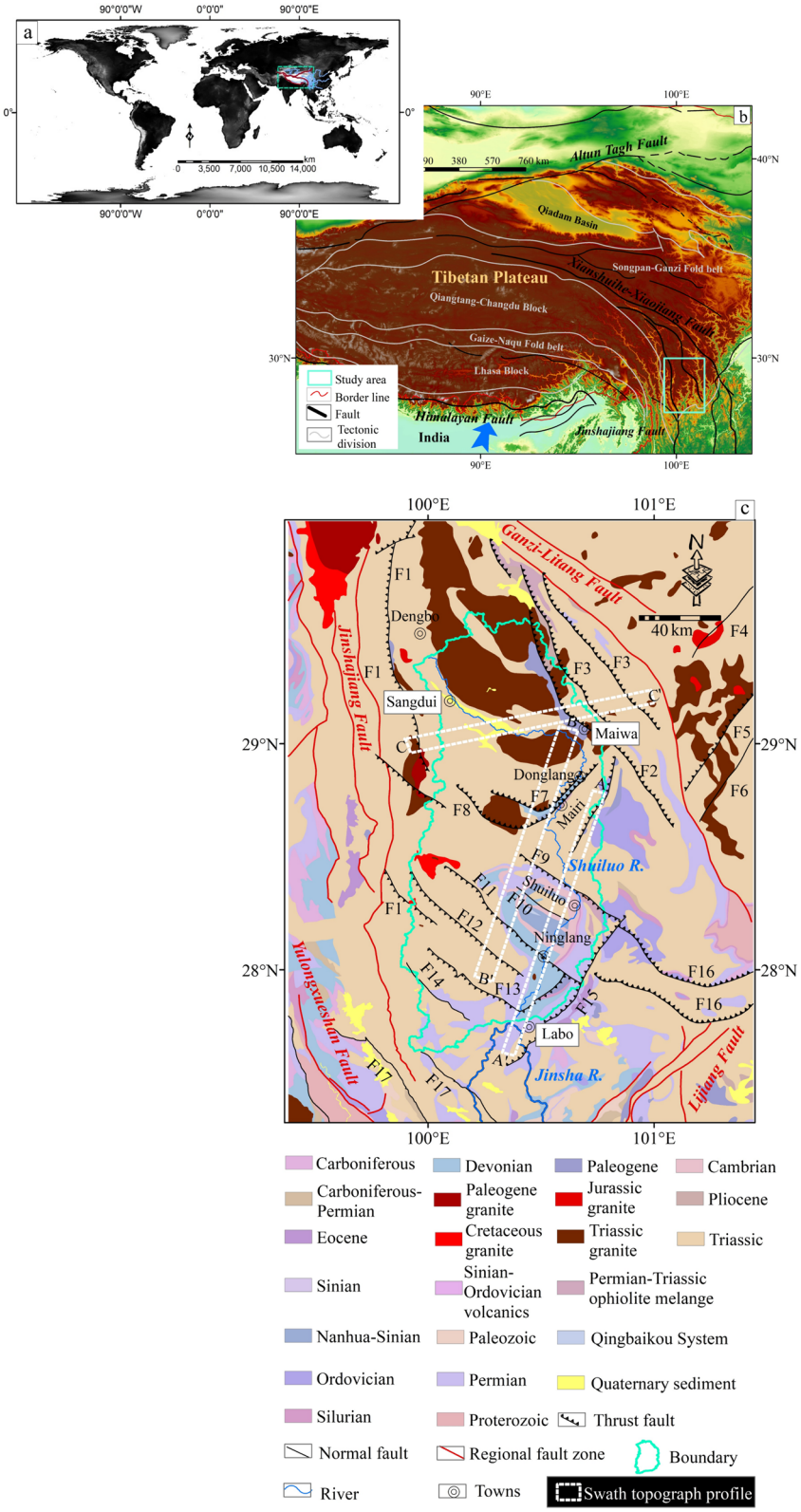

Fig. 1 (See legend on previous page.)

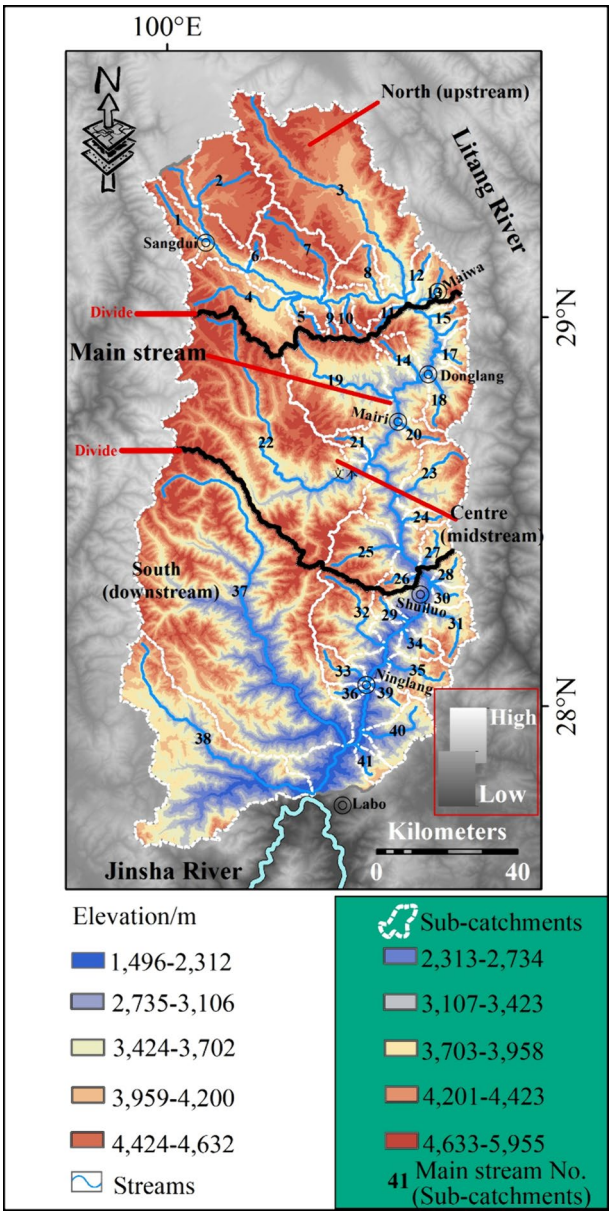

Fig. 2 Elevation reclassification and basic landform types of SRC. Elevation reclassification of SRC and name of these tributaries. Note: all tributaries' names and informations see Table 1

Table 1 Informations of main streams in each sub-catchment

Stream no	Name	Stream length (km)	Catchment area(km^2)
1	Riyong	26.24	133.22
2	Balongqu	18.48	415.79
3	Niqingqu	88.05	1309.78
4	Banghe	39.57	406.22
5	Nadingchuogou	18.49	53.01
6	Hecuogou	12.24	30.84
7	Zajiaogou	40.00	260.57
8	Zeyong	21.58	116.32
9	Reying	10.72	21.43
10	Nayingyongbao	15.10	46.75
11	Darongqu	12.79	33.92
12	Zhangjianyong	17.10	44.84
13	Gonggongyong	16.43	120.94
14	Gonggenggou	20.37	75.63
15	Morong	9.40	39.72
16	Cuohong	8.19	21.10
17	Zengdonggou	9.77	64.40
18	Xironghe	18.04	173.50
19	Lanyaohe	41.04	580.61
20	Dasigonggou	14.98	57.89
21	Zirong	14.90	40.40
22	Chituhe	98.91	1789.48
23	Watuogou	26.26	266.27
24	Gedehen	12.80	46.76
25	Baishuihe	22.16	276.26
26	Siwenggou	12.21	47.06
27	Luoduogou	14.91	80.46
28	Wolonggou	12.89	61.56
29	Yanmushudu	12.87	42.99
30	Luodouhe	11.00	46.18
31	Qunyinggou	22.29	143.63
32	Lapaigong	33.22	305.43
33	Rangjiegong	19.12	86.01
34	Shawabugou	13.38	67.62
35	Quanmaguaigou	20.58	146.05
36	Xiaqiaohe	10.22	36.49
37	Chongtianhe	126.14	2977.56
38	Niruhe	78.67	1186.45
39	Duocaihe	11.39	45.89
40	Yijigou	24.41	173.24
41	Saduogou	11.80	53.24

where h_{mean} indicates the value of the average elevation in a region, h_{min} indicates the minimum elevation, and h_{max} indicates the maximum elevation.

3.2 Asymmetry factor (AF)

Asymmetry factor (AF) is used to evaluate the degree of tectonic inclination in a certain basin. The *AF* index value could characterize the degree of tectonic tilt of a basin. The value of $|AF\text{-}50|$ is generally defined to quantitatively reveal the tectonic activity in a catchment. In other words, the greater the absolute value, the greater the degree of tectonic tilt in a basin, and the greater the inclination of a basin trunk toward the left or right bank. Generally speaking, when $AF < 7$, the tectonic inclination is low; when $7 \leq AF < 15$, the tectonic inclination is moderate; when $AF \geq 15$, the tectonic inclination is large, and

a basin is strongly affected by tectonic activity (Hare and Gardner 1985; Pérez-Peña et al. 2010). And the calculation formula is:

$$AF = \frac{Ar}{At} \times 100 \tag{2}$$

where Ar indicates the area on the right side of a certain watershed flowing along the main stream and At is the total area (Hare and Gardner 1985; Cox 1994).

3.3 Basin Shape Ratio (BS)

Basin shape ratio (BS) is used to quantitatively evaluate the shape of a watershed. The *BS* index represents the development shape of a basin. The larger the *BS* value, the narrower basin shape. The smaller the *BS* value, the wider the basin shape. When $BS \geq 3$, the basin shape is very narrow, and the intensity of tectonic activity is extremely strong, additionally, the surface uplift is in the initial stage. When $2 \leq BS < 3$, the basin shape is in the transition stage from narrow to broad, and the tectonic activity is relatively strong. When $BS < 2$, the basin shape gradually becomes wider, and it is in the stage of geomorphic evolution dominated by external force erosion, and the tectonic activity is relatively weak (Bull and Mcfadden 1977) the calculation formula is:

$$BS = \frac{Bl}{Bw} \tag{3}$$

where Bl indicates the maximum length of the watershed, Bw indicates the maximum width of the watershed.

3.4 Valley floor width–valley height ratio (VF)

The *VF* value can reflect the shape of the valley. If the *VF* value is large, the valley shape is U-shaped. If the *VF* value is small, the valley shape is wide V-shaped or deep V-shaped. The *VF* value can generally indicate the intensity of tectonic activity. The deep canyon ($VF<0.50$) shows that the tectonic uplift is intense and the erosion basis is decreased and the stream erosion direction is mainly down-cutting. The river valley becomes wider and the stream erosion direction is mainly lateral and the tectonic activity is moderate when $0.50 \leq VF < 1.00$. When $VF>1.00$, the river valley is U-shaped or wide U-shaped, the stream gradually stopped cutting down and laterally eroded to both sides, which is a stage of weak tectonic activity (Bull and Mcfadden 1977). The formula is:

$$VF = \frac{2Vfw}{(ELd - Esc) + (Erd - Esc)} \tag{4}$$

where Vfw is the width of the valley floor, Esc is the height of the valley floor, Eld is the elevation value of the left shoulder of the valley, and Erd is the elevation value of the right shoulder of the valley (facing downstream).

3.5 Normalized channel steepness index (k_{sn})

Under natural conditions, the relationship between the slope of the *stream channel* (S) and the *drainage area* (A) follows a power-law function (Flint 1974; Sklar et al. 1998; Snyder et al. 2000), namely:

$$S = k_s \cdot A^{-\theta} \tag{5}$$

where k_s is the steepness index of the stream, indicating the degree of steepness of the stream channel; θ Represents the concavity coefficient of a river channel, reflecting the degree of concavity of the stream channel (Whipple 2004). In a steady state, using the hydraulic erosion model of bedrock rivers (Whipple and Tucker. 1999):

$$E = KA^m S^n \tag{6}$$

The power-law function relationship can be obtained:

$$S_e = (U/K)^{1/n} A^{-m/n} \tag{7}$$

In Eqs. (6) and (7), E is the erosion rate of the river, S_e is the slope of the stream in equilibrium state, U is the rate of rock uplift, K is the dimensional erosion coefficient, and K value mainly reflects the effects of climate, lithology, structure and other factors (Whipple and Tucker 1999; Snyder et al. 2000). m and n are constants. Comparing Eqs. (5) and (7), when the river is in equilibrium state, there are:

(See figure on next page.)

Fig. 3 The swath topography profile in the SRC. We try to select a range that spans as many stratigraphic units as possible to create swath topography profile. We have created three swath topography profile (A–A′, B–B′, and C–C′) spanning upstream, midstream, and downstream, displaying the maximum, minimum, and average elevation values of the swath coverage area, enabling the most intuitive observation and analysis of the terrain. The blue arrow refers to the stream, corresponding to its number. The red arrow indicates a fault. The green straight line represents the boundary of stratigraphic lithology. Note: T: Triassic limestone; E: Paleogene conglomerate; P: Permian limestone; H: clastic rocks with carbonate rocks in the Xiajiang Formation of the Cambrian-Ordovician; D: Devonian schist and marble; TH: Triassic granite; NHZ: moraine conglomerates and volcanic clastic rocks of Nanhua-Sinian Mulipingwumuzuo Formation; Q: Quaternary sediment; SRM: main stream of Shuiluo River; JSR: Jinshan River; SM: Snow mountain

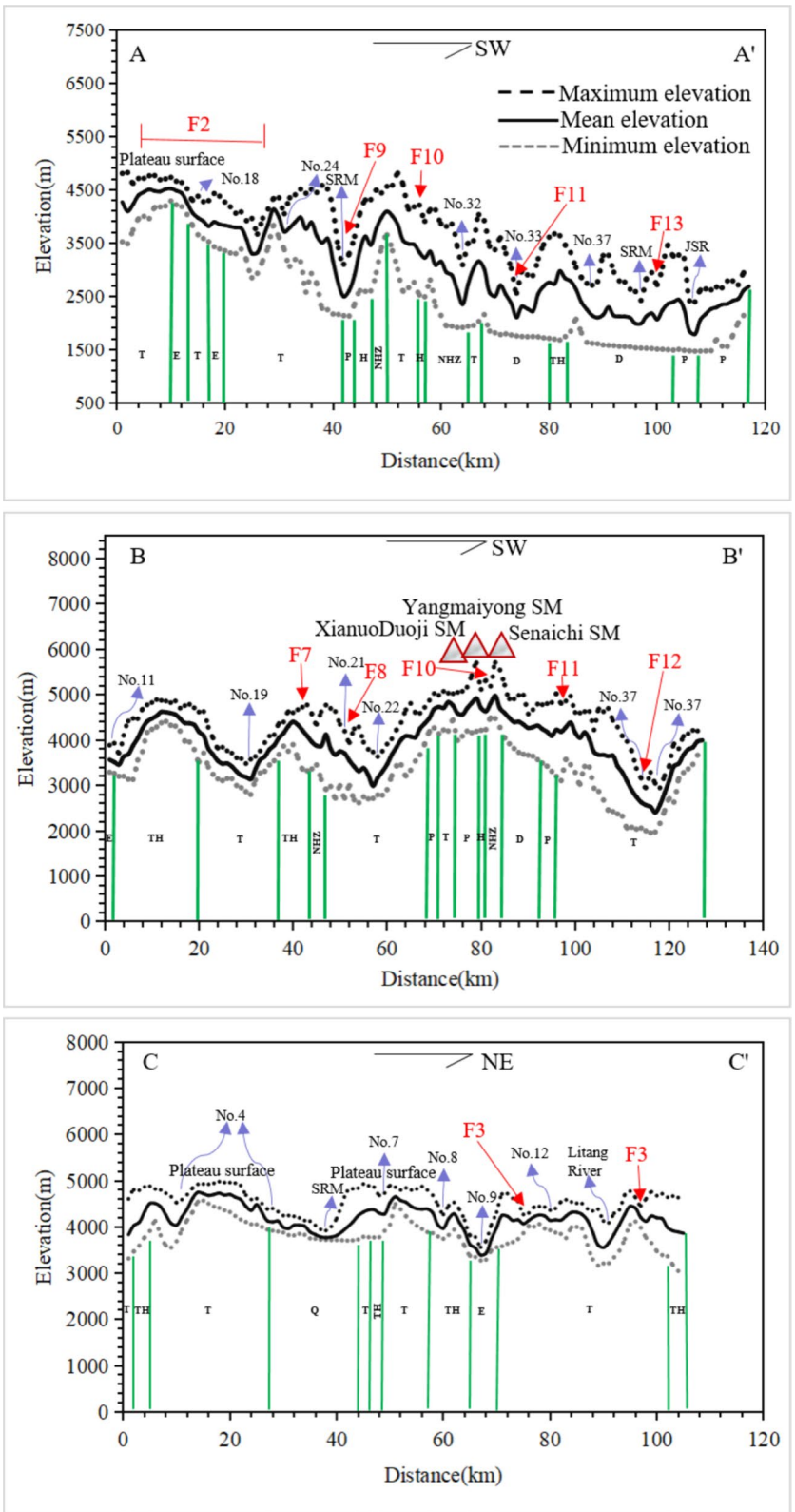

Fig. 3 (See legend on previous page.)

$$k_s = (U/K)^{1/n} \tag{8}$$

and:

$$\theta = m/n \tag{9}$$

Due to the varying basin sizes of streams, in order to compare streams with different basin sizes, a reference depression value can be taken, i.e the θ^{ref}=0.45 is used to calculate the standardized steepness coefficient of streams (Wobus et al. 2006):

$$S = k_{sn} \cdot A^{-\theta ref} \tag{10}$$

In Eq. (10), the longitudinal profile of a stream in equilibrium presents a smooth concave state, and the degree of steepness of its longitudinal profile is represented by the *normalized channel steepness index* (k_{sn}). The logarithmic relationship between the stream slope and the catchment area is a straight line, and its intercept (a parameter representing the overall slope of the stream) can be used to reflect the tectonic-climate interaction (Howard and Kerby 1983; Howard et al. 1994). In an instantaneous state, the stream longitudinal profile is generally divided into sections of different steepness by a knickpoint, which is the turning point at which the river section is divided into different slopes on the stream longitudinal profile (Kirby and Whipple. 2012). The steepness of a stream longitudinal profile can reflect rich information on tectonic. After site investigation, the study area developed bedrock channels or bedrock alluvial mixed channels, which met the k_{sn} extraction requirements.

3.6 Index of relative active tectonics (RIAT)

The *RIAT* is obtained by calculating the geomorphic parameters value of each sub-catchment. Then we divided the *RIAT* following the classification of above six parameters of each sub-catchment (Table 2) (Alipoor et al. 2011; Hare and Gardner 1985; Bull and Mcfadden 1977). Grade 1 ($1.0 \leq RIAT < 1.5$) represents that tectonic activity is very strong; grade 2 ($1.5 \leq RIAT < 2.0$) represents that tectonic activity is strong; grade 3 ($2.0 \leq RIAT < 2.5$)represents that tectonic activity is moderate; grade 4 ($RIAT \geq 2.5$) represents that tectonic activity is weak (Hamdouni et al. 2008). The classification of various geomorphic parameters and the division of *RIAT* can see table 2, which also lists the reference and basis for division (Table 2). *RIAT* is calculated as follows:

$$RIAT = \left(HI_{grade} + AF_{grade} + BS_{grade} + VF_{grade} + k_{sngrade}\right)/5 \tag{11}$$

4 Results

4.1 *HI* and *HI* curve

The spatial distribution of *HI* index in SRC shows that the range of *HI* values in this basin is 0.41–0.71, and the spatial range varies greatly. For comparison, the *HI* values of SRC are divided into three grades. The first level is $0.61 \leq HI \leq 0.71$; the second level is $0.51 \leq HI \leq 0.60$; the third level is $0.41 \leq HI \leq 0.50$. The spatial distribution map shows that the first level is mainly in the midstream and downstream in the SRC, and north bank of the upstream. The second level occupies a large area of midstream and downstream. The third level is only distributed in a few sub-catchments on the south bank of the upstream of Shuiluo River's mainstream (Fig. 4a). We used the CaIHypso (Pérez-Peña et al. 2010) to obtain the *HI* curve of each sub-catchment in the SRC. The results show that most of the curves are convex or S-shaped, and only the *HI* curves of sub-catchments 1 and 4 are concave (Fig. 4b). These two subcatcahments are also the regions with the lowest *HI* values in the SRC (No. 1 is 0.41; No. 4 is 0.45). The *HI* value of SRC is generally high and the average value is 0.59, and most sub-catchments landforms reach. This indicates that the SRC tectonically activity is generally strong.

4.2 *AF* and tectonic tilt direction

The spatial distribution of *AF* values in each sub-catchment of SRC shows that the spatial variation range of *AF* value is 1.21–30.09. According to the inclination classification method constructed by *AF* index, we divided the *AF* value of SRC into 3 grades. The first grade is $15.00 \leq AF < 30.09$; the second grade is $7.00 < AF < 15.00$; the third grade is $1.21 \leq AF \leq 7.00$. Among them, the first level is mainly in SRC's midstream and downstream, with a large area; the level 2 is mainly distributed in the upper reaches, while it in the middle and lower is scattered; the level 3 is mainly located in the intersection of the midstream and downstream of the studied basin, and the distribution area is very small. The degree of tectonic tilt in the upstream of the SRC varies irregularly (Fig. 5a). The sub-catchments in the midstream and downstream generally incline from south to north (most of the sub-catchments in the west bank tilt to the left bank, and the east bank mainly tilt to the right bank) (Fig. 5b). The squeezing effect of the Tibetan Plateau's uplift results in the overall tilt uplift of its periphery from east to west or from south to north, which is consistent with the tectonic uplift of the SRC.

4.3 BS

The *BS* value of the SRC varies from 0.25 to 2.99. The sub-catchments with *BS* values ranging from 0.25 to 1.00 are mainly distributed on the left bank of the upstream,

Table 2 Classification method of tectonic activity grade of various geomorphic parametres

	Grade 1	Grade 2	Grade 3	Grade 4	References
HI	HI ≥ 0.50	0.40 ≤ HI < 0.50	HI < 0.40	–	Alipoor et al. (2011)
AF	| AF-50 | ≥ 15	7 ≤ | AF-50 | < 15	| AF-50 | < 7	–	Pérez-Peña et al. (2010)
BS	BS ≥ 3	2 ≤ BS < 3	BS < 2	–	Bull et al. (1977)
VF	VF < 0.50	0.5 ≤ VF < 1	VF ≥ 1	–	Hamdouni et al. (2008)
k_{sn}	296.78 ≤ k_{sn} ≤ 504.86	156.76 ≤ k_{sn} ≤ 296.77	54.64 ≤ k_{sn} ≤ 156.75	–	Xu et al. (2016)
RIAT	1 ≤ RIAT < 1.5	1.5 ≤ RIAT < 2	2 ≤ RIAT < 2.5	2.5 ≤ RIAT	Hamdouni et al. (2008)

the left bank of the midstream and the right bank of the downstream (No. 38 sub-catchment), the basin area accounts for only 21.00 % of the total area; the sub-catchments with *BS* values ranging from 1.01 to 1.99 are distributed in most areas of the SRC, accounting for 57.98 %; the sub-catchments with BS values ranging from 2.00 to 2.99 are less distributed, mainly located in the intersection of the upper and middle reaches, and in the downstream of the study area, the basin area only accounts for 20.58 % (Fig. 6)

4.4 VF

In a catchment, as the main stream represents the erosion basis of the region relative to its tributaries, the main stream is the region that is most sensitive to the response of tectonic and climate processes in the catchment (Chang et al. 2015; Fan et al. 2018). The evolution of valleys is also the region with the most significant feedback on regional tectonic deformation and uplift in fluvial geomorphology. Therefore, based on the above theory, we calculated the *VF* index of 41 sub-catchments in SRC. We calculated the *VF* values of the mainstream and tributaries of Shuiluo River at a sampling interval of 6km, and obtained the *VF* average values for each sub-catchment. The results show that the river valleys with *VF* >1.00 are mainly in the north of the studied basin; deep V-shaped canyons with *VF* < 0.50 and *VF* < 0.10 are mainly scattered among middle and south of SRC. The average values of *VF* index of the sub-catchments in SRC also show that the low *VF* values are scattered among midstream and downstream of the SRC (Fig. 7).

4.5 k_{sn} and stream profile

The stream power incision model shows that the stream longitudinal profile of the bedrock channel in the active tectonic zone is mostly in an disequilibrium state. And the stream profile in an unbalanced state usually has upper convex reaches (knickpoint). Knickpoint divides the longitudinal profile of the stream into sections with different steep indices (k_{sn}). The larger the k_{sn} value, the steeper the stream longitudinal profile develop, which usually indicate the tectonic or climate change along the stream longitudinal profile. This method of judging the steepness of the stream longitudinal section to reveal the tectonic informations contained in the active zone has been widely used in the field of tectonic geomorphology. According to the methods provided by previous work, we used GIS system and MATLAB script program to extract data like drainage basin and elevation from DEM, and we set 250m as the smoothing window to smooth the channel and took 12.2m as the elevation interval and set the reference concavity (θ^{Ref}) as 0.45 according to Eq. (10). Finally, we extracted the longitudinal profile, log SA and k_{sn} of the mainstream and 41 tributaries of the SRC, and determined the location of the knickpoints based on the longitudinal profile of the stream (Whipple and Tucker 1999; Snyder et al. 2000; Kirby et al. 2003). At the same time, we calculated the k_{sn} average values of 41 sub-catchments of SRC. The results of k_{sn} index are divided into 3 grades according to the natural split point discontinuity method (the first level is 296.78–504.86; the second level is 156.76–296.77; the third level is 54.64–156.75) (Fig. 8a, b). The results show that most of the streams in the SRC are in transient state, and they developed multiple knickpoints. The high k_{sn} values are mainly scattered among the lower sections of the midstream, and in downstream of the SRC. The low values are mainly in the upper sections of midstream and in upstream of SRC (Fig. 8a), such as No. 1–19 streams. More knickpoints are developed in the midstream and downstream (such as Nos. 22–37) than in the upstream, which indicates that the longitudinal profile of the stream in the midstream and downstream of the SRC is steeper (Fig. 9).

Since the χ value can be used to determine the stability of catchment watershed (Whipple 2004), we extracted the χ value of SRC and its surrounding streams. The results showed that there was a significant difference in the χ value between the left watershed boundary of SRC and the midstream of Jinsha River, indicating a migration toward SRC. However, there was no significant difference in the χ value of the stream source between the first level sub-catchments within SRC watershed. And there is no significant difference in χ values compared to other external watersheds, such as the Litang River on the right side

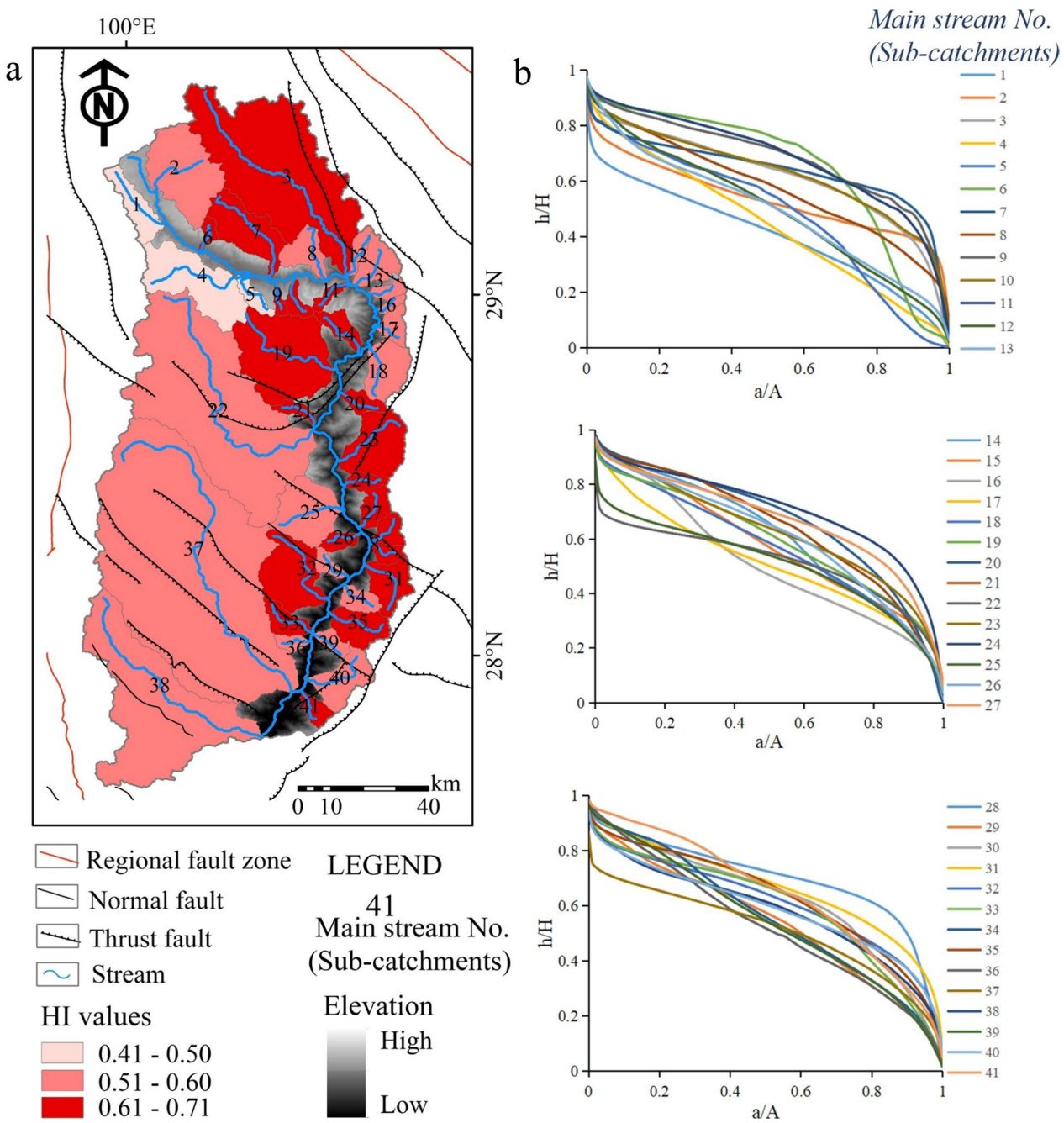

Fig. 4 **a** The distribution map of *HI* values in SRC, **b** *HI* curve diagram. Note that in the horizontal axis of the curve, "*a*" represents the area above a certain contour line in the watershed. "*A*" represents the area of the entire watershed; on vertical axis "*h*" is the height difference between a certain contour line and the lowest point of the watershed, and "*H*" is the height difference between the highest point and the lowest point of the entire watershed

of SRC. Therefore, the χ value of SRC is not affected by inter catchment erosion and migration, and the watershed is relatively stable. In addition, we also extracted the local k_{sn} values of all streams within and around the SRC watershed. Note that the extracted stream k_{sn} values here are not only the k_{sn} values of the trunk channels of the primary tributaries of each catchment, but also the local k_{sn} values of all streams. This is to more intuitively display the spatial differences in k_{sn} values of the SRC catchment and its surrounding streams. The results show that the k_{sn} values in the midstream and downstream of the watershed are generally higher, while those in the upstream are

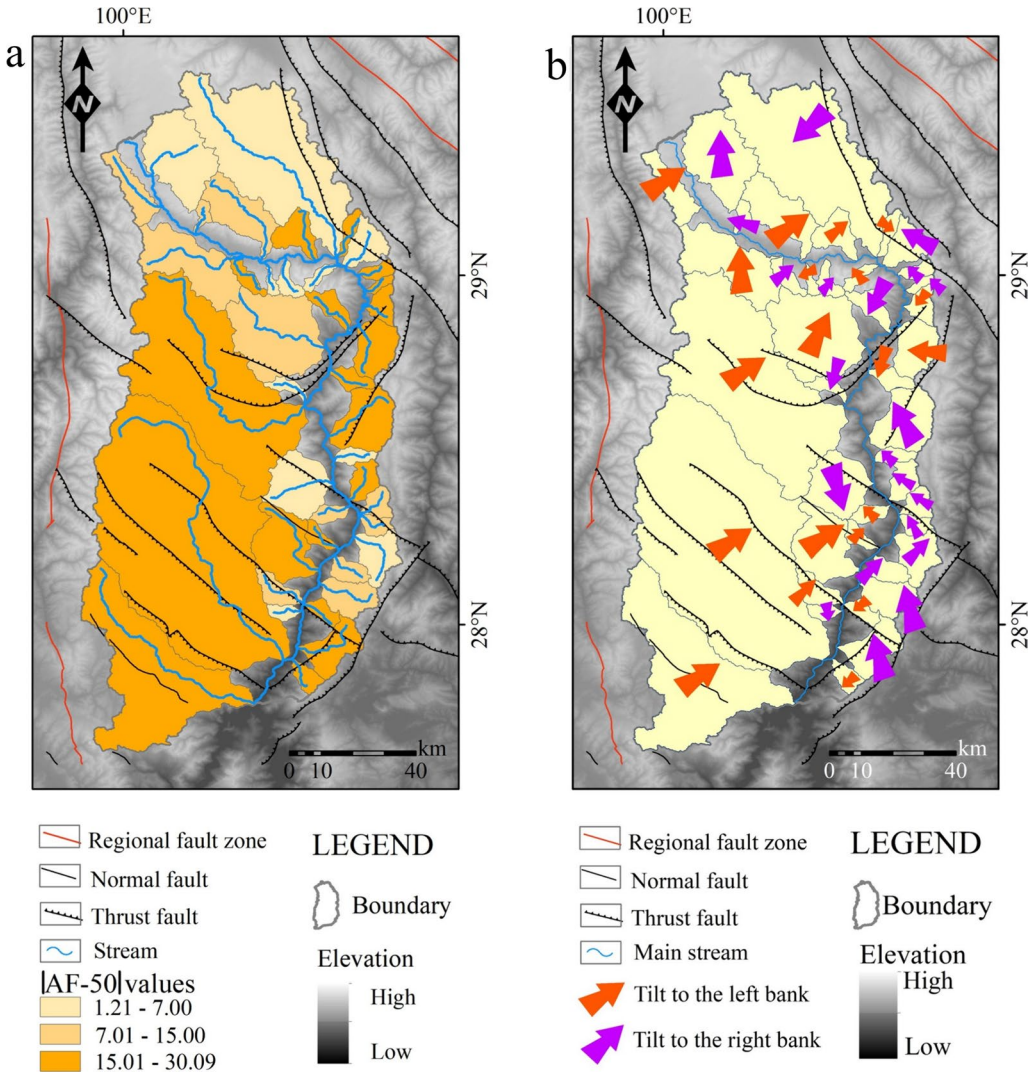

Fig. 5 **a** The distribution of | *AF-50* | index values in SRC, **b** tectonic tilt direction

smaller. This is consistent with the extracted k_{sn} values of the trunk channels of the 41 sub-catchments in the SRC. All phenomena indicate that the k_{sn} values in the middle and downstream of the SRC are high while those in the upstream are low, and the watershed between the sub-catchments within the SRC is relatively stable(Fig. 10a, b).

4.6 RIAT

Based on the results of the geomorphic parameters we extracted, we calculated the *RIAT* of each sub-catchment in the SRC according to the classification method of tectonic activity levels of each geomorphic parameter (Tables 2, 3), and divided different tectonic activity levels (Fig. 11) with different colors in the GIS system. Our results show that there are very few sub-catchments with the first level (1.00–1.49), only No. 27 (Luoduogou) and No.32 (Lapaigong) sub-catchments in the midstream exist in the first level. The level 2 (1.50–1.99) are distributed in the center and south of the SRC. The level 3 (2.00–2.49) are mainly scattered among the lower sections of the upstream in Shuiluo River, and the distribution area is very small. The level 4 (2.50–2.83) is in the northwest of the SRC. Therefore, the SRC's intensity of tectonic activity is characterized by low in the north and high in the central and south generally.

5 Field geological work

We conducted necessary field work to verify the consistency between the extraction results of fluvial geomorphic parameters and the field geology and geomorphology. We found many extremely wide valleys in upstream of SRC, which are distributed on the plateau surface upstream of

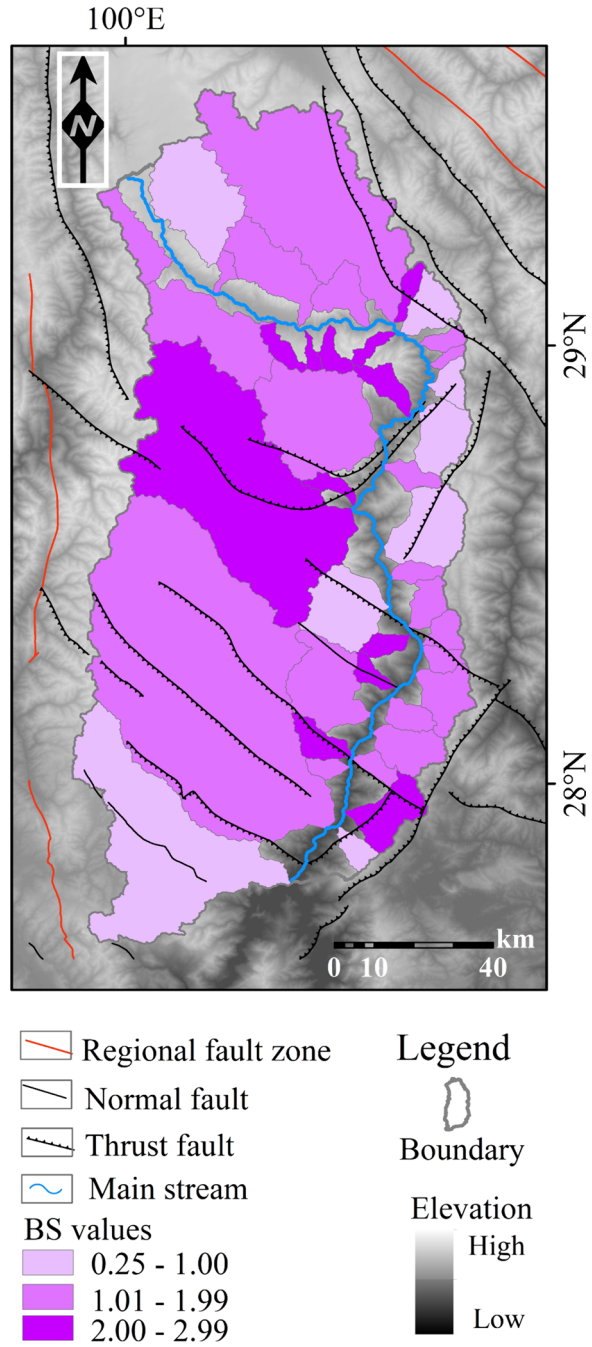

Fig. 6 The distribution of *BS* index values of SRC

SRC. Their common characteristics are widely developed wide valleys and low undulating topography (Fig. 12a–d). On the contrary, extremely deep canyons have developed in the midstrea, and downstream, distributed on highly undulating topography (Fig. 12e–j). In addition, we have observed landslides and fault (Fig. 12k, l) in some areas of the midstream and downstream.

In addition, we conducted cross domain investigations on the upstream, midstream, and downstream areas of SRC and found that the upstream streams are generally wide and gentle, flowing on the flat plateau surface (Fig. 12m–n). In the midstream and downstream of SRC, extremely steep stream channels are generally developed, and there are many knickpoints. These channels are developed on the extremely steep and steep topography in the midstream and downstream of SRC. We have found these commonly developed steep fluvial sections (Fig. 12o–u) on some large tributaries such as Chituhe, Lanyaohe, and Chongtianhe in the midstream and downstream of SRC. The extremely significant topographic differences in the up, mid, and downstream of SRC are products of differential tectonic activities, which may be controlled by differential uplift on the southeastern edge of the Tibetan Plateau. This differential uplift may create spectacular landscape of low undulating plateau surfaces and high undulating mountain gorges on the southeastern edge. Our field investigation results are consistent with the geomorphic parameters and the index of relative tectonic activity of the division, indicating that our DEM based geomorphic research on SRC region is reliable.

6 Discussion

6.1 Factors affecting the geomorphological evolution of Shuiluo River Catchment

The evolution of geomorphology is restricted by internal and external forces such as climate, lithology, glaciation and tectonic (Cyr et al. 2014). The lithology and tectonic of SRC are complex and are affected by glaciation in some areas (Roughly located within the range of 100.25°E–100.50°E, 28.35°N–28.40°N). These glacier is modern glaciers, mainly developed since the Quaternary period. Therefore, for the interior of the catchment, the impact of glaciers on the overall geomorphic evolution of the study area can be ignored. In terms of climate, SRC belongs to the temperate plateau climate zone, but the south is wholly in the subtropical monsoon climate, so there are certain differences in climate. Therefore, climate is also an important factor that cannot be ignored when analyzing the geomorphic evolution of the SRC.

6.1.1 Climate (precipitation) and glaciation

In the process of stream erosion, precipitation plays a vital role. The greater the precipitation, the stronger the stream erosion capacity, the shorter the time for the landform evolution to the middle and old age stage. When the precipitation is small, the external erosion becomes weak, the geomorphic evolution is still in the early stage (Snyder et al. 2000). We collected the average precipitation (mm/a) of the SRC in the past 30 years from 1991 to 2020 (https://psl.noaa.gov/data/gridded/data.UDel_

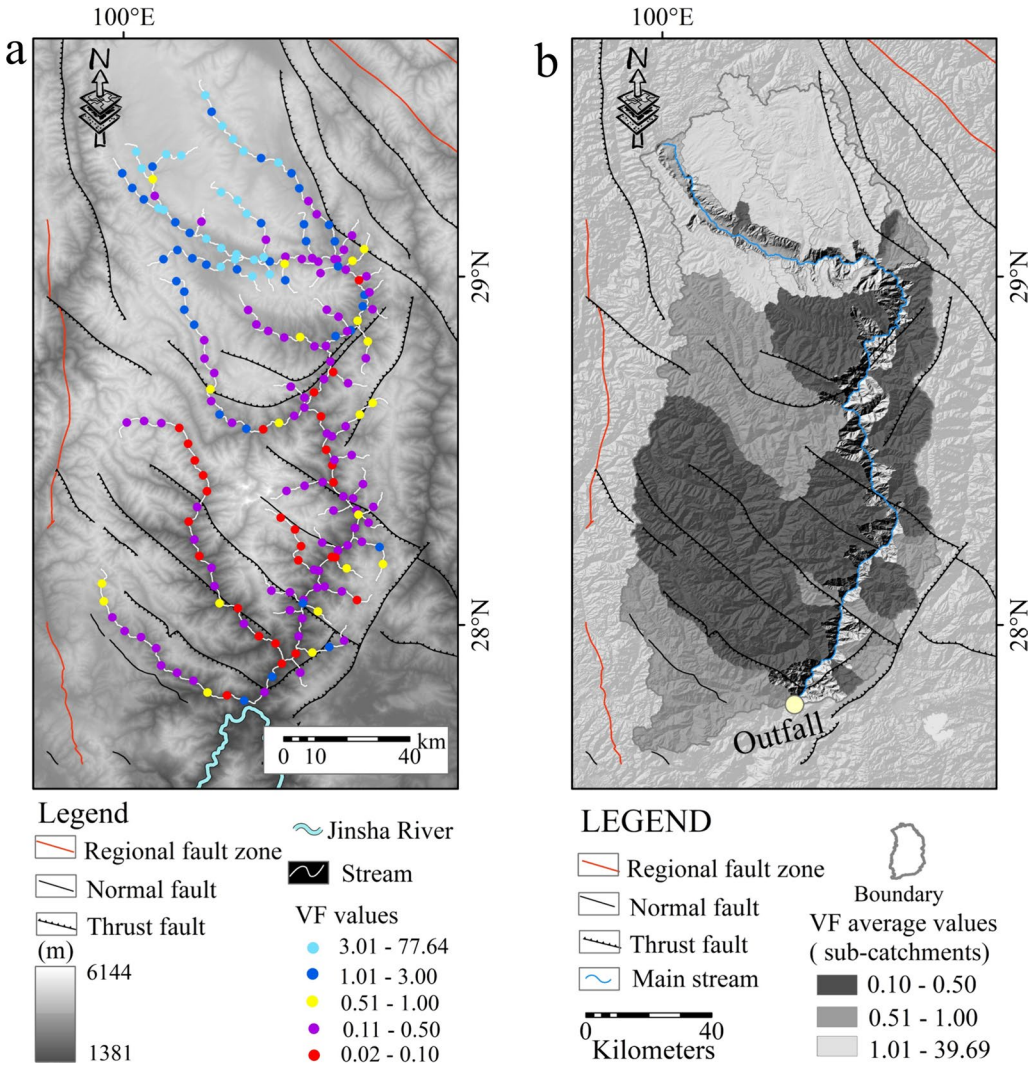

Fig. 7 **a** The spatial distribution map of *VF* values in SRC, **b** average *VF* values of 41 sub-catchments in the study area

AirT_Precip.html). We superimposed this data through the GIS system and re-classified it to obtain the annual average precipitation distribution map of the SRC (Figs. 13, 14). Figure 13 shows that the precipitation range of the SRC is 630.1-814.6 mm/a, and the precipitation is generally high in the south and low in the north. The rainfall in the southeast, south and central parts is relatively large, while the rainfall in the north and northwest is relatively small. This is inconsistent with the spatial distribution characteristics of various geomorphic parameter values and the level of activity tectonic in SRC. In addition, the correlation coefficients between various geomorphic parameters and rainfall are relatively small (R^2<0.6) (Fig. 14). Therefore, precipitation is not the main factor affecting the landform index of SRC.

There is a difference in erosion efficiency between glacier erosion and stream hydraulic erosion. In the area affected by glaciers, the valley is generally U-shaped. Especially for the stream power incision model, due to the difference in erosion efficiency, the boundary between glacier erosion and stream erosion usually forms a knickpoint, which is an important basis for exploring the causes of stream knickpoints in glacier distribution areas (Chen et al. 2018). We collected the glacier data (http://www.ncdc.ac.cn/portal/) and used it to study the relationship between the geomorphic evolution and glacial processes of SRC. The spatial distribution of glaciers in the SRC indicates that large-scale glaciers are concentrated in the Minya Konka in Kangding, and Litang in Ganzi Prefecture. Inside the SRC, it is mainly located in the middle of the basin, near the Daocheng Yading Scenic Spot (Fig. 13). The distribution of glaciers in study area is less, which only influences local areas. For the whole basin, glaciers are not the main influencing factors of

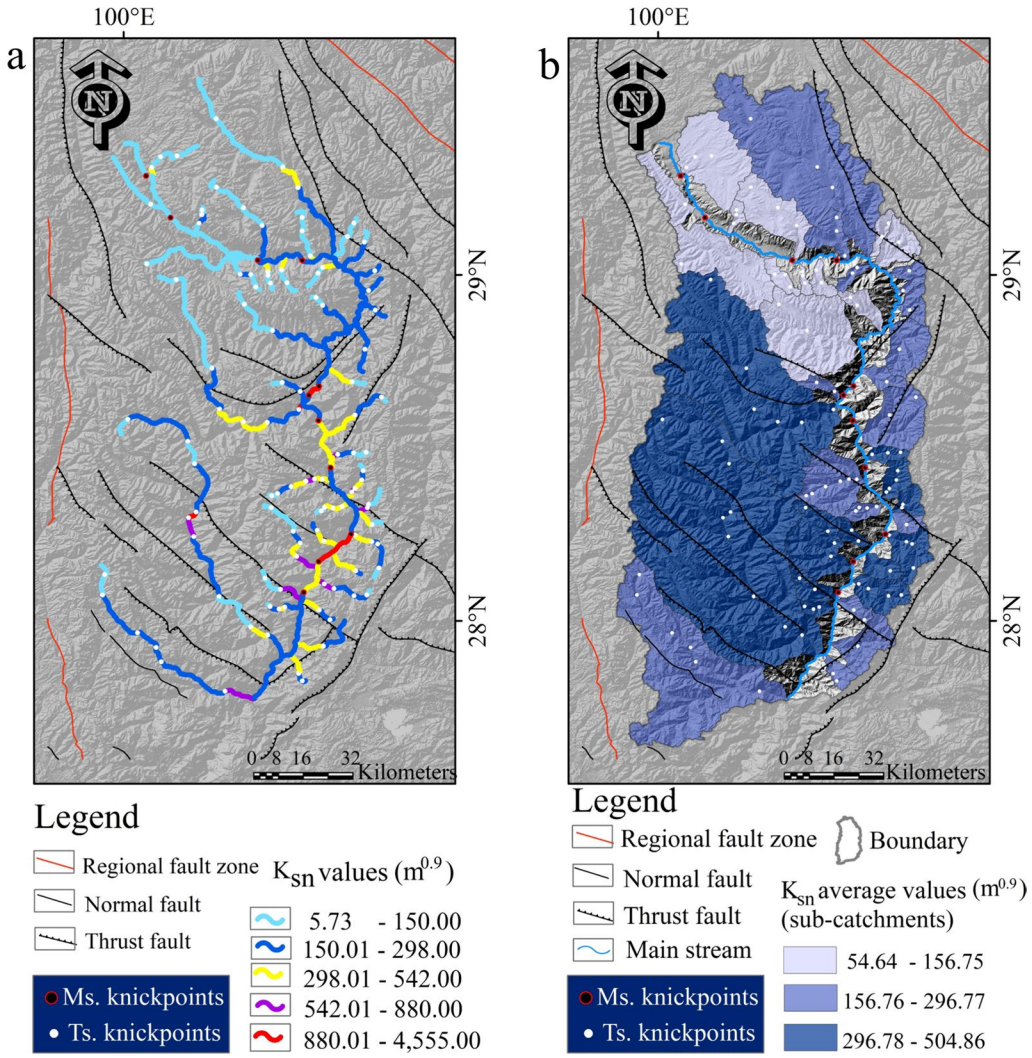

Fig. 8 **a** Spatial distribution of k_{sn} values and knickpoints in SRC, **b** spatial distribution of k_{sn} average values in 41 sub-catchments of SRC. Ms.knickpoints represent knickpoints developed on the main stream. Ts. knickpoints represent knickpoints developed on tributaries

geomorphic evolution. In addition, the catchment area has a certain impact on geomorphic parameters. However, we found that the linear fitting of the sub-catchment area and geomorphic parameters of SRC showed poor fit (R^2 <0.1). Therefore, the impact of basin area on the values of geomorphic parameters is also limited (Fig. 15)

6.1.2 Lithology

The impact of lithology on geomorphic evolution is mainly reflected in its erosion resistance. The stronger the erosion resistance, the higher the grade of the geomorphic index. The weaker the erosion resistance, the older the landform development, and the lower the corresponding level of landform index. In theory, hard rocks are more resistant to erosion and weathering, while soft rocks are more susceptible to weathering (Bahrami et al. 2015). We divide the bedrock of Shuiluo River Catchment into hard rock, relatively hard rock, relatively soft rock, soft rock and extremely soft rock according to the soft and hard degree of the rock following to "Geological engineering handbook." Igneous rocks and granites are hard rocks; sandstone, limestone, biological limestone, dolomite and marble are relatively hard rocks; moderately weathered metasandstone, slightly weathered slate, phyllite and pyroclastic rock are relatively soft rock; slightly weathered shale, argillaceous sandstone and mudstone are soft rocks; semi-consolidated glutenite, conglomerate and Quaternary deposits are extremely soft rock. Based on the above theory, we classified rocks of various lithology, and used different colors in GIS to represent the spatial distribution of bedrock hardness and softness (Fig. 16).

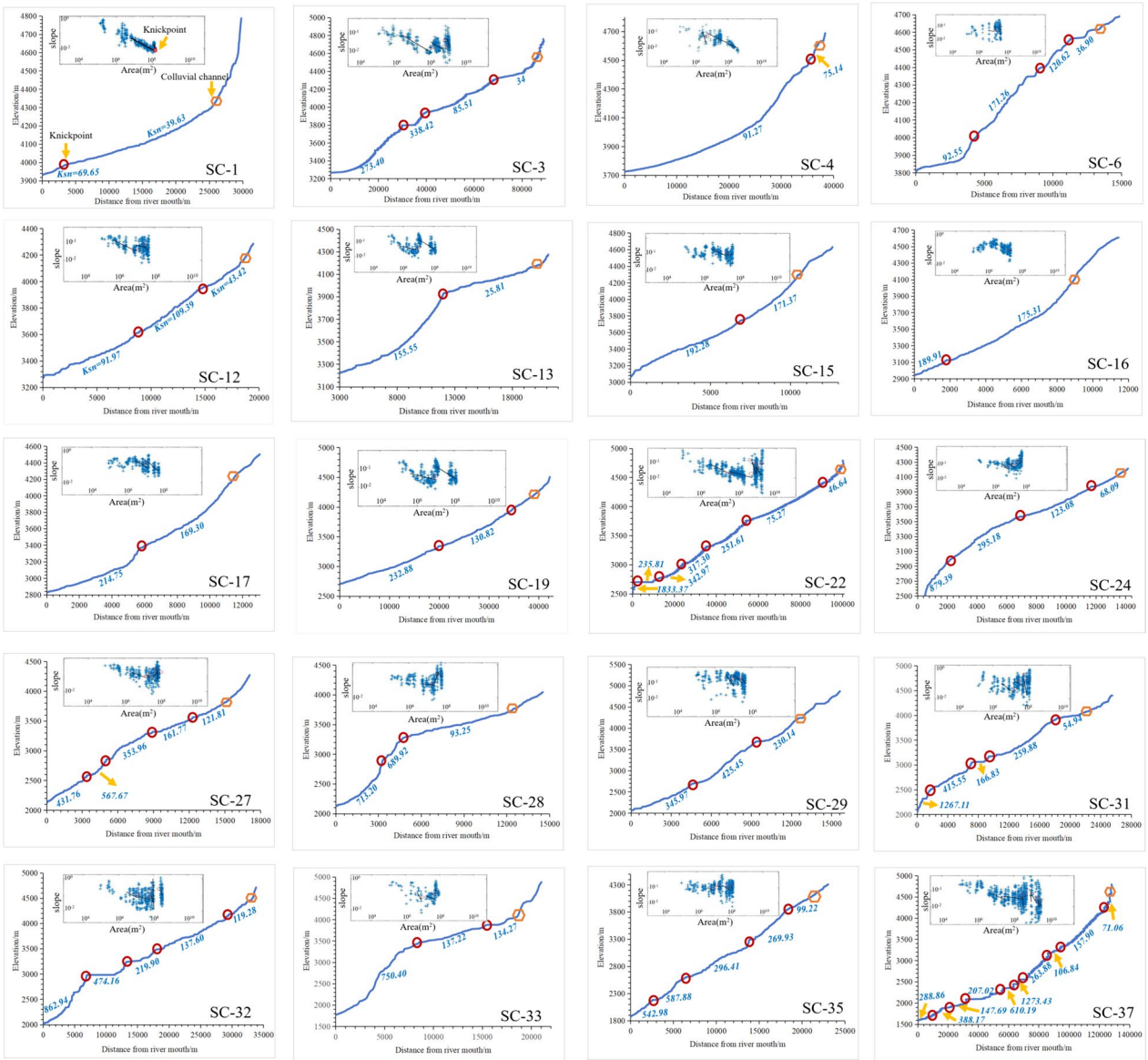

Fig. 9 Stream longitudinal profile and area-slope logarithmic diagram (log SA) of some stream sections of SRC. No. 1–19 are the stream longitudinal profile and log SA of the tributaries in the upstream and upper of the midstream. It is obvious that the stream longitudinal profile in this area is relatively not steep and the k_{sn} index values are low, and the number of developed knickpoints are small. No. 22–37 are the river longitudinal profile and log SA of the tributaries in the midstream and downstream. The stream longitudinal profile in this area is steep and the k_{sn} values are high, and the number of developed knickpoints is also large

The result shows that there are mainly relatively hard rock and relatively soft rock in most areas of the SRC. The relatively soft rock is mainly in the west and center of SRC and the relatively hard rock is mainly distributed in the center and south. In addition, hard rock is mainly distributed in the north of the basin and the left bank of the upstream of mainstream. The soft rock and extreme soft rock are only distributed in the north and central part of the basin, and the distribution area is small. The geomorphic index of study area shows that the level of geomorphic parameters in the northern part of the basin is generally lower, and the level of geomorphic parameters in the midstream and lower downstream is higher (Figs. 16, 17), which is inconsistent with the spatial distribution of bedrock erosion resistance. Therefore, on the whole, the development and evolution of the landform of the SRC has little relationship with the lithology of the bedrock.

However, since the *VF* and k_{sn} values of SRC can better reflect the response of local area (stream reach) to

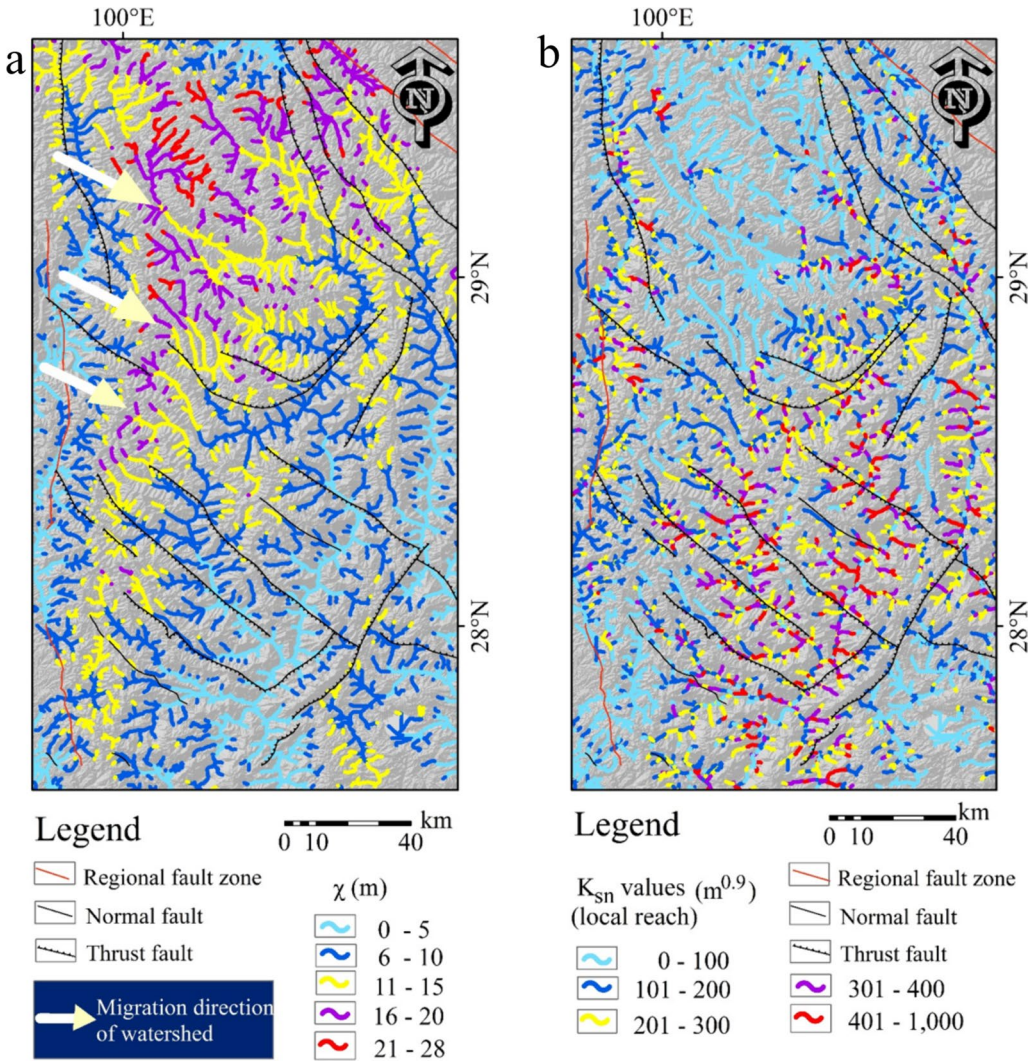

Fig. 10 The χ and k_{sn} values of SRC and its surrounding streams. **a** χ values; **b** local k_{sn} values

lithology, it is a question to further discuss whether the geomorphic evolution is affected by the erosion resistance of bedrock in local area. Therefore, we will discuss these two index values separately. First of all, the grades of *VF* and k_{sn} average values in each sub-catchment of SRC are obviously high in the middle and south and low in the north (Figs. 7, 8). This is not consistent with the spatial distribution of bedrock erosion resistance (Figs. 16, 17). Therefore, on the whole, The strength of bedrock is not the main controlling factor influencing the *VF* and k_{sn} average values of the basin. Secondly, we found that the local *VF* and k_{sn} values are inconsistent with the spatial distribution of bedrock strength as a whole. For example, the k_{sn} values of partial stream segments (Nos. 3, 7 and 10 sub-catchments) transit from hard rock to relatively hard rock, relatively soft rock or extremely soft rock, the k_{sn} values becomes larger (Fig. 16a), this is contrary to the theory that the stronger the rock strength, the higher the k_{sn} values (Cyr et al. 2014). Although overall, rock strength is not the main factor controlling the geomorphic parameters of the study area, we found that geomorphic evolution processes related to changes in rock strength can still be observed in some regions (or stream sections). For example, some knickpoints develop at the boundary of rock strength, but there are no large-scale knickpoints that produce this phenomenon. So we will systematically point out the geomorphic parameter values related to lithological changes. For the *VF* value, these measurement points in the river valley transition from soft rock to hard rock, with the *VF* value decreasing and the river valley narrowing from width, as follows: Nos. 2–3, 12–13; The measurement points for valleys that transition from hard rock to soft rock, where the *VF* value

Table 3 Fluvial geomorphic parameter values and their grades

Sub-catchments' codes	HI values	HI grade	| AF-50 | values	| AF-50 | grade	BS values	BS grade	VF values	VF grade	k_{sn} values	k_{sn} grade	RIAT values	RIAT grade
1	0.41	3	13.34	2	1.56	3	2.38	3	54.64	3	2.80	4
2	0.54	2	4.59	3	0.55	3	7.03	3	150.57	3	2.80	4
3	0.62	1	6.57	3	1.82	3	2.13	3	182.91	2	2.40	3
4	0.45	3	7.25	2	1.37	3	4.32	3	88.43	3	2.80	4
5	0.48	3	15.12	1	2.70	2	39.69	3	78.67	3	2.40	3
6	0.65	1	7.54	2	1.70	3	0.48	1	150.33	3	2.00	3
7	0.64	1	11.66	2	1.95	3	7.18	3	93.63	3	2.40	3
8	0.58	2	24.84	1	1.17	3	1.22	3	176.95	2	2.20	3
9	0.68	1	2.29	3	2.99	2	5.77	3	132.40	3	2.40	3
10	0.63	1	3.84	3	2.28	2	1.23	3	156.75	3	2.40	3
11	0.68	1	1.21	3	2.56	2	1.52	3	221.15	2	2.20	3
12	0.50	2	15.95	1	2.61	2	0.4	1	81.59	3	1.80	2
13	0.50	2	3.64	3	0.84	3	0.78	2	90.68	3	2.60	4
14	0.60	1	20.69	1	2.09	2	0.31	1	141.72	3	1.60	2
15	0.58	2	18.51	1	1.86	3	0.2	1	181.83	2	1.80	2
16	0.51	2	20.31	1	1.92	3	0.33	1	182.61	2	1.80	2
17	0.51	2	30.09	1	0.63	3	0.2	1	192.03	2	1.80	2
18	0.57	2	27.35	1	0.85	3	0.47	1	188.03	2	1.80	2
19	0.60	1	10.01	2	1.05	3	0.38	1	145.32	3	2.00	3
20	0.67	1	15.59	1	1.65	3	0.18	1	240.50	2	1.60	2
21	0.64	1	6.53	3	2.62	2	0.2	1	227.55	2	1.80	2
22	0.51	2	19.13	1	2.04	2	0.83	2	443.28	1	1.60	2
23	0.62	1	19.47	1	0.97	3	0.4	1	228.12	2	1.60	2
24	0.71	1	2.63	3	1.96	3	0.18	1	341.44	1	1.80	2
25	0.51	2	6.24	3	0.94	3	0.25	1	292.74	2	2.20	3
26	0.61	1	10.06	2	2.04	2	0.16	1	296.77	2	1.60	2
27	0.67	1	16.97	1	1.80	3	0.18	1	327.39	1	1.40	1
28	0.70	1	11.41	2	1.19	3	0.46	1	498.79	1	1.60	2
29	0.54	2	16.65	1	2.43	2	0.36	1	367.19	1	1.40	1
30	0.62	1	9.26	2	1.77	3	0.12	1	255.36	2	1.80	2
31	0.67	1	4.51	3	1.56	3	0.77	2	504.86	1	2.00	3
32	0.61	1	26.23	1	1.29	3	0.1	1	362.78	1	1.40	1
33	0.60	1	13.96	2	2.18	2	0.52	2	340.66	1	1.60	2
34	0.56	2	9.34	2	1.70	3	0.42	1	319.93	1	1.80	2

Table 3 (continued)

Sub-catchments' codes	HI values	HI grade	| AF-50 | values	| AF-50 | grade	BS values	BS grade	VF values	VF grade	k_{sn} values	k_{sn} grade	RIAT values	RIAT grade
35	0.63	1	10.62	2	1.58	3	0.14	1	359.29	1	1.60	2
36	0.53	2	3.42	3	1.85	3	0.18	1	308.56	1	2.00	3
37	0.51	2	19.55	1	1.89	3	0.17	1	342.62	1	1.60	2
38	0.58	2	20.50	1	0.94	3	0.55	2	249.42	2	2.00	3
39	0.55	2	26.44	1	1.95	3	0.61	2	276.17	2	2.00	3
40	0.59	2	20.87	1	2.33	2	0.83	2	279.38	2	1.80	2
41	0.65	1	25.16	1	1.00	3	0.37	1	275.03	2	1.60	2

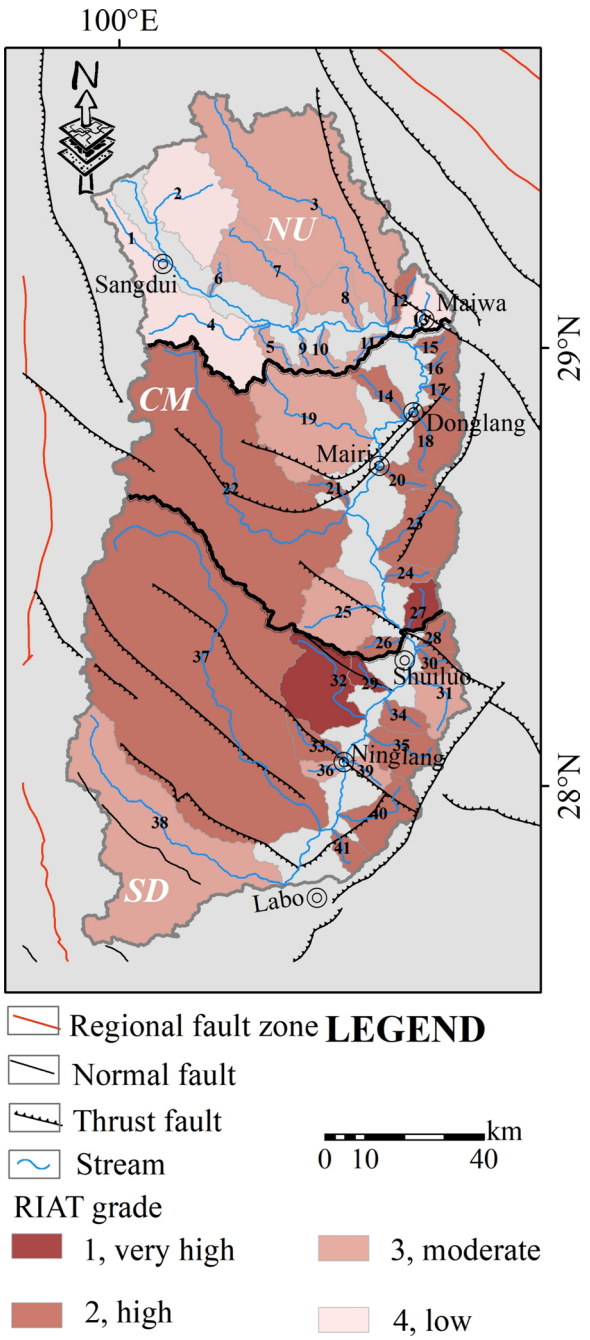

Fig. 11 The *RIAT* spatial distribution map of SRC. Note that the thick black lines in the figure represent the boundary between upstream, midstream, and downstream, that is, the boundary between the north, middle, and south. NU: North (upstream); CM: Center (midstream); SD: South (downstream)

changes from low to high, and the river valley changes from narrow to wide are Nos. 18–19. Nos. 5–11 flows through soft Quaternary sediments, and the valley is generally wide, while Nos. 14–18 passes through hard rock covered areas, with low *VF* values and deep valleys (Figs. 18, 19, 20). Large number of faults developed in valleys below No. 24. Thus these valleys below are deep V-type, and the *VF* values have not changed significantly. Even on some lithological boundaries, the *VF* values are always low (Figs. 18, 19, 20), which shows that only in the upper part of the upstream and mainstream of SRC and the local area of the midstream, the *VF* value is affected by the rock strength. For the k_{sn} values, the values are related to lithological changes in the midstream of sub-catchments Nos. 22, 23, and 40, as well as the upstream and downstream reaches of Nos. 31, 37 and 39 (Fig. 16). The spatial distribution of knickpoints has a poor correspondence with the spatial distribution of rock erosion resistance (there is no large area of knickpoints developed on the boundary of rock hardness and softness) (Fig. 16). Therefore, overall, the differences in rock strength only affect partial regions, and the geomorphic evolution of the study area is weakly correlated with lithology.

6.1.3 Tectonics

A series of NW-SE faults, such as Xisashi, Boke, Qiasi, Langlang, Guaishaoti, Lagenwa, Yangta Fault, and a series of NE-NW faults, such as Zhangke, Zhongdian-Xiangcheng Fault, have been developed in study area. Mengzi Fault and Chitu Fault deflected from NW to NE at the main stream of Shuiluo River. The distribution of these faults within the SRC mainly presents a spatial distribution feature of dense in the central and southern regions and dispersed in the northern regions, and most of these faults are thrust faults with generally strong activity (Hao et al. 1990; Tang et al. 1993; Xu et al. 2016) . Therefore, we speculate that this may be a significant factor in the difference in SRC activity between the central southern region and the northern region (Figs. 21, 22). In addition, a series of regional fault zones, such as Jinshajiang, Ganzi-Litang, Yulongxueshan and Lijiang, are also developed around the SRC (Fig. 1b, c). The regional geological structure system is extremely complex. The differential activity of faults is possible and important factor affecting the geomorphic evolution. The spatial distribution of active faults in SRC is highly consistent with the geomorphic parameters. After excluding climate, glacier, and lithological factors, it can be estimated that fault activity is the possible and main controlling factor affecting the geomorphic evolution of the study area. Although we have confirmed above that the *VF*, and k_{sn} values of some stream sections are related to lithological changes, overall, tectonic activity is still considered the most significant factor affecting the geomorphic evolution of the study area. As for the influence of tectonic factors on k_{sn} value and knickpoint, the stream reaches on both sides of the fault or across the fault usually form a knickpoint,

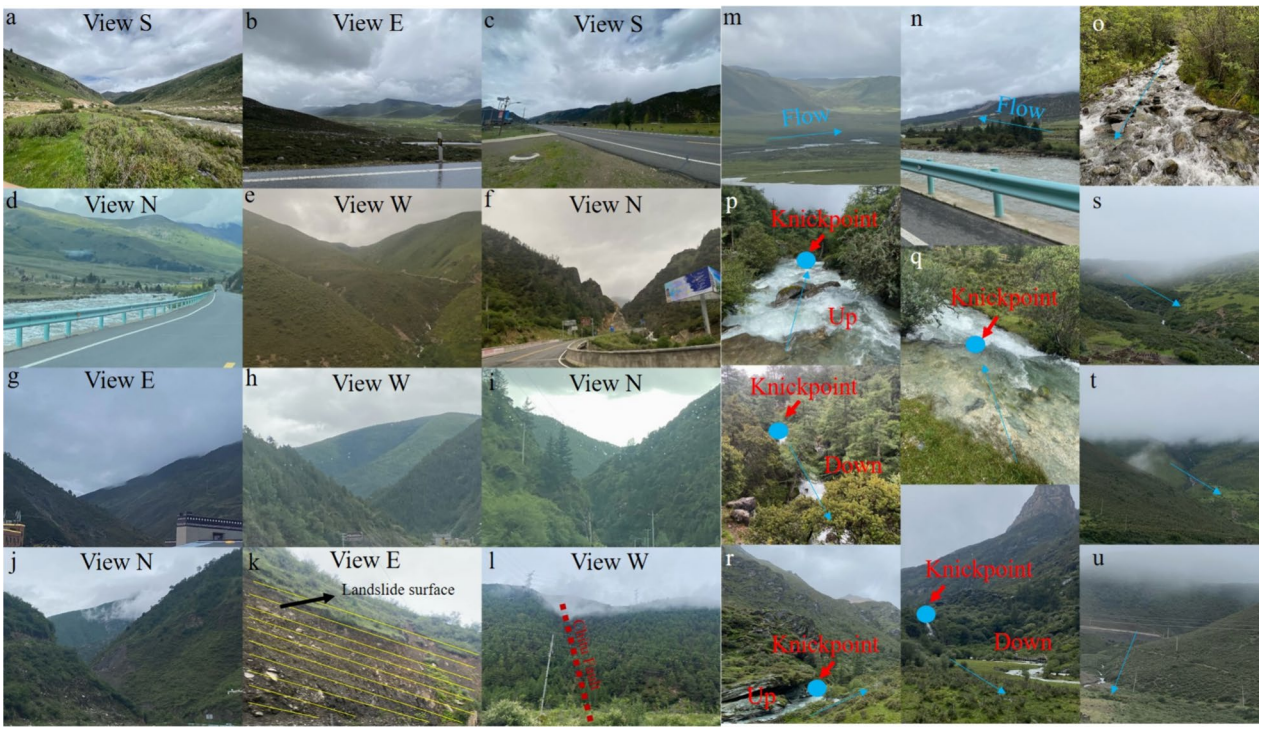

Fig. 12 **a** wide valley developed on the left bank tributary of Niqinqu (No. 3 stream) in the north of SRC, **b** a wide valley at the source of Niqinqu river, **c** a low undulating terrain in the upstream of SRC, **d** a wide valley between Sangdui and Maiwa in the upstream of SRC, **e** a narrow valley on the right bank tributary in the middle reaches of Chituhe (No. 22 stream), **f** a V-shaped valley in the middle reaches of Chituhe main stream, **g** a V-shaped valley downstream of Chituhe main stream, **h**–**i** some V-shaped valleys developed in the midstream of Chituhe main stream, **j** a V-shaped valley developed downstream of SRC's main stream, **k** Landslides developed downstream of Chituhe, **l** a thrust fault developed in the middle of Chituhe, **m** gentle fluvial channels near Niqinqu at the northern end of SRC, **n** a gentle fluvial upstream of the main stream of n SRC, **o** steep channels developed in the midstream of Chituhe, **p**–**r** steep fluvial sections near the right bank tributary of Chituhe, and developed knickpoints, **s**–**t** steep fluvial sections developed upstream of Lanyaohe (No.19 stream), **u** a steep fluvial section developed on the tributary of u Chongtianhe (No. 37 stream)

and the difference of k_{sn} value in the stream reaches above and below the knickpoint will become more significant accordingly. However, among the 41 streams in the study area, many of the knickpoints developed on the streams did not cross the fault zone. However, the erosion base level decrease and the sudden increase of rock mass uplift rate caused by tectonic uplift will also produce corresponding tectonic knickpoints, and such tectonic knickpoints will move upstream with time (migrating knickpoint) (Cyr et al. 2010; Wang et al. 2020). Therefore, we believe that even though there is no good corresponding relationship between the knickpoint and the fault, the tectonic activity is still the main factor for the generation and development of the river knickpoint in most rivers in the study area after the exclusion of glacier, precipitation, lithology and other factors. Weirs caused by landslides and debris flows also produce convex split points on the fluvial longitudinal profile of rivers. After field observation of most rivers in the study area, we find that the influence of weirs is extremely limited, and this factor can be excluded.We collected the seismic activities of magnitude 2–5 in the study area from 2000 to 2022. The seismic distribution map in the study area shows that earthquakes mainly occurred in the midstream and downstream of the basin, and in the upper reaches, only two earthquakes of magnitude 2–3 occurred near Sangdui. In contrast, earthquakes in the midstream and downstream occurred more frequently and with larger magnitude (Fig. 22). This is consistent with the geomorphic parameter values and the spatial distribution of the tectonic activity level we extracted. The spatial distribution of The *RIAT* in the sub-catchment of SRC also shows that the downstream tectonic activity is stronger, which may indicate that the fault activity developed in the downstream is stronger. The (U-Th)/He low-temperature thermochronology data of detrital apatite and zircon along the periphery of the study area indicate that differential tectonic uplift occurred in different parts of the SRC (Lai et al. 2007; Tian et al. 2014; Gourbet et al. 2019). In particular, the thermal history of the Zhongdian Massif,

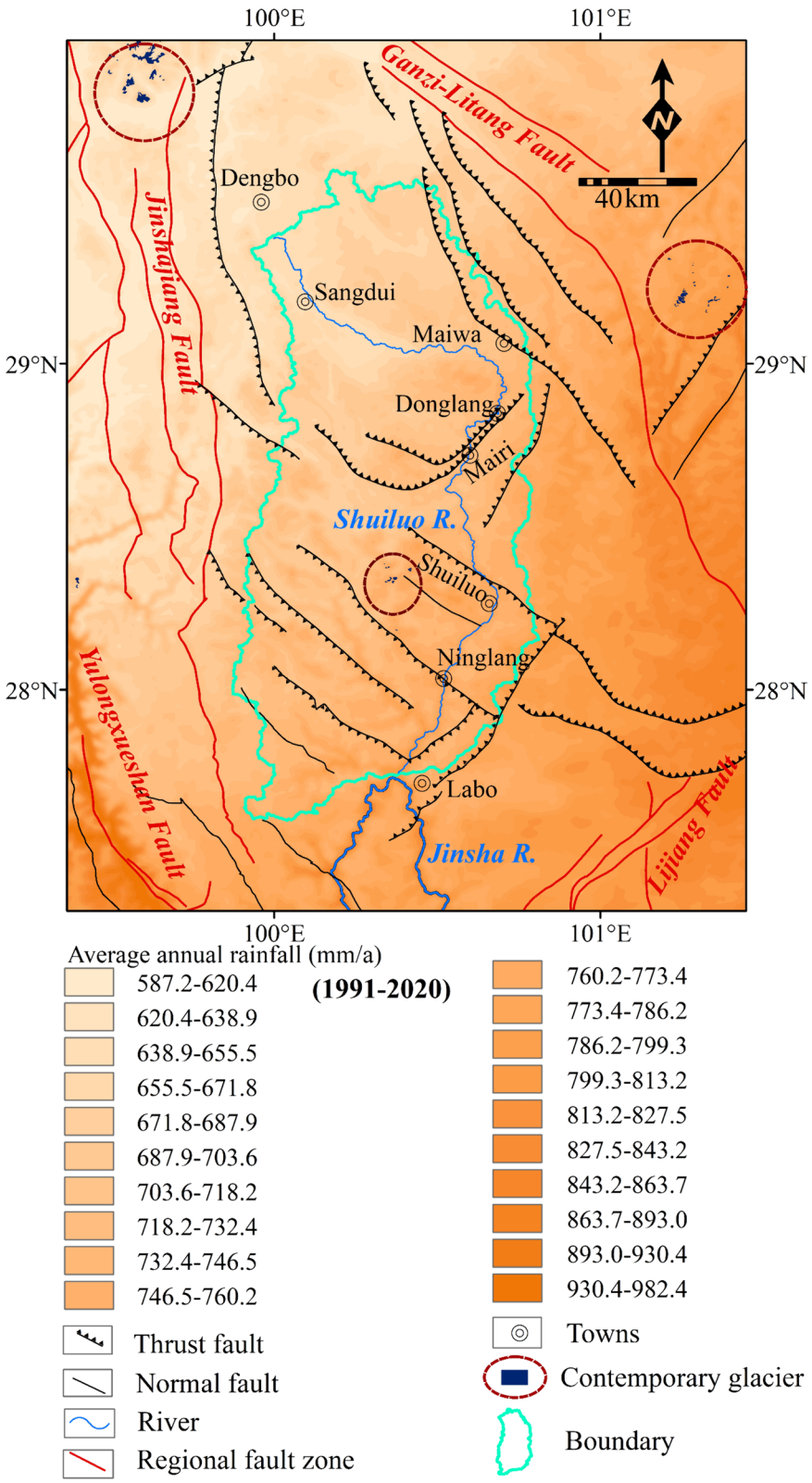

Fig. 13 The spatial distribution of precipitation in SRC from 1991 to 2020 (https://www.esrl.noaa.gov/psd/data/), glacier data were obtained from http://www.ncdc.ac.cn/portal/. It can be clearly seen that the area of glaciers in the SRC is only in the center, near the Aden scenic area in Daocheng

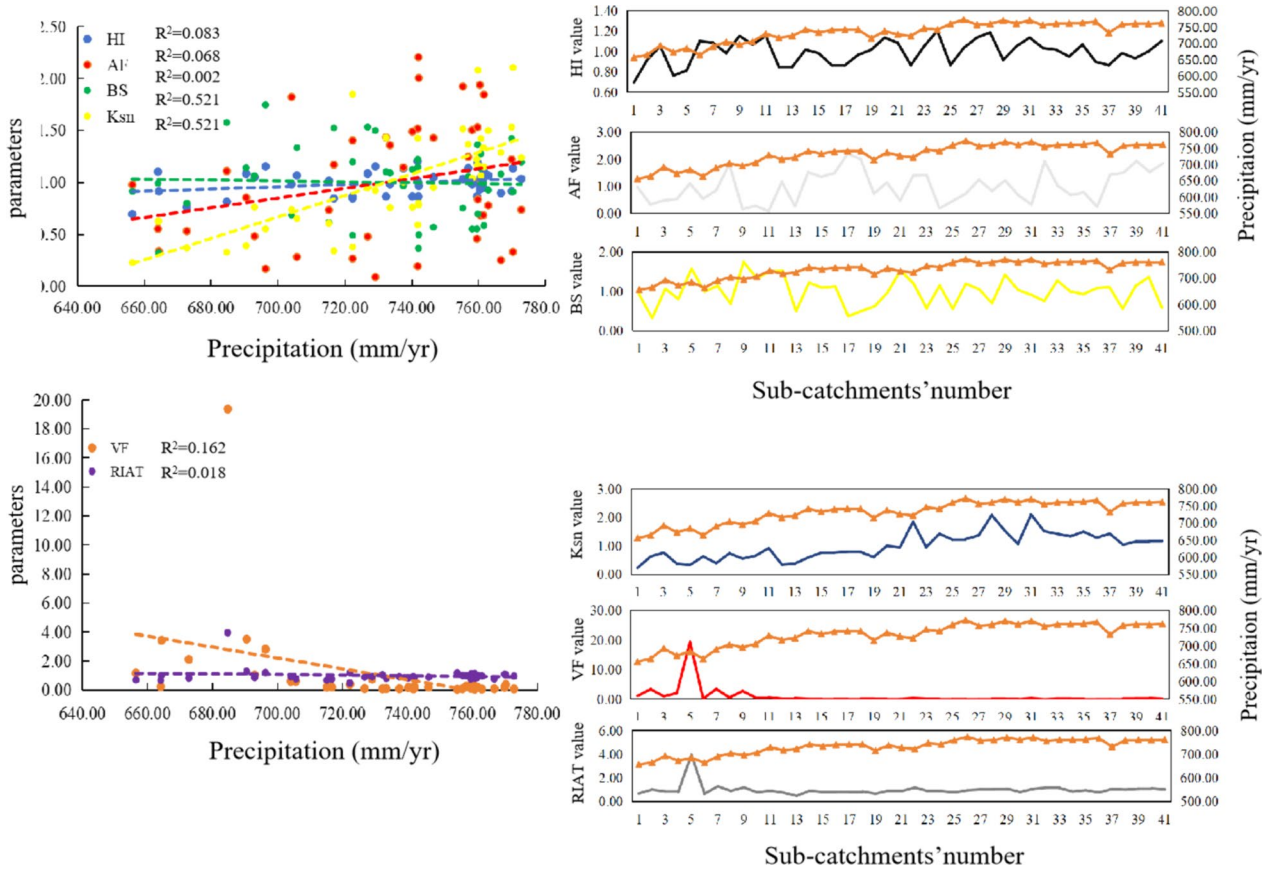

Fig. 14 The correlation coefficient graph between rainfall and various geomorphic parameters (on the left side of the above figure); and distribution map of the rainfall and various geomorphic parameters (right)

which is located downstream, suggests that all samples experienced rapid uplift during the Pliocene. The tectonic uplift is mainly concentrated in two time periods, namely 5.2–10.2 Ma and 5.2 Ma. The impact of the tectonic uplift process since 5.2 Ma has been significant. The influence of 5.2 Ma is quite extensive. This confirms that since 5.2 Ma, the tectonic denudation rate of the Zhongdian block had been rapid, reaching 213.3 m/Ma–226.7 m/Ma suggesting that the central and south part of the study area as a whole may have experienced faster tectonic uplift than the north since the Pliocene. In contrast to this is the relatively earlier uplift and lower denudation ration in the north part of the study area (Zou et al. 2014). This is consistent with the fact that the southeastern margin of the Tibetan Plateau experienced little denudation during the Late Cretaceous to Early Miocene, resulting in a geomorphic surface with low elevation and low relief. In downstream of SRC, near the Jinsha River valley, the motion field captured by Global Navigation Satellite System (GNSS) shows a higher movement rate (Wang and Shen 2020), which may be related to the dextral strike slip in the middle and lower sections of the Jinshajiang Fault. Anyway, this seems to point to a conclusion that there may be high tectonic activity intensity in the middle or downstream of SRC (Fig. 22).

To sum up, geological structure (fault system) and tectonic uplift are the leading factors affecting the development and evolution of the geomorphology of SRC. Affected by the tectonic system and differential tectonic uplift, the tectonic activities in the upstream, and upper section of the midstream of the SRC are relatively weak. The tectonic activity in the lower section of the midstream, and the downstream are strong, and the tectonic activity in the downstream is the strongest, which may be related to the differential activities of the faults in the two regions. In the upper section of the upstream and upper part of the midstream, exist partial stream sections the geomorphic evolution is affected by the difference of rock erosion resistance. We extracted the fluvial geomorphological indexes to quantify the landform development and activity tectonic intensity of SRC. The level of the geomorphic parameters and the *RIAT* are relatively consistent with the regional seismic

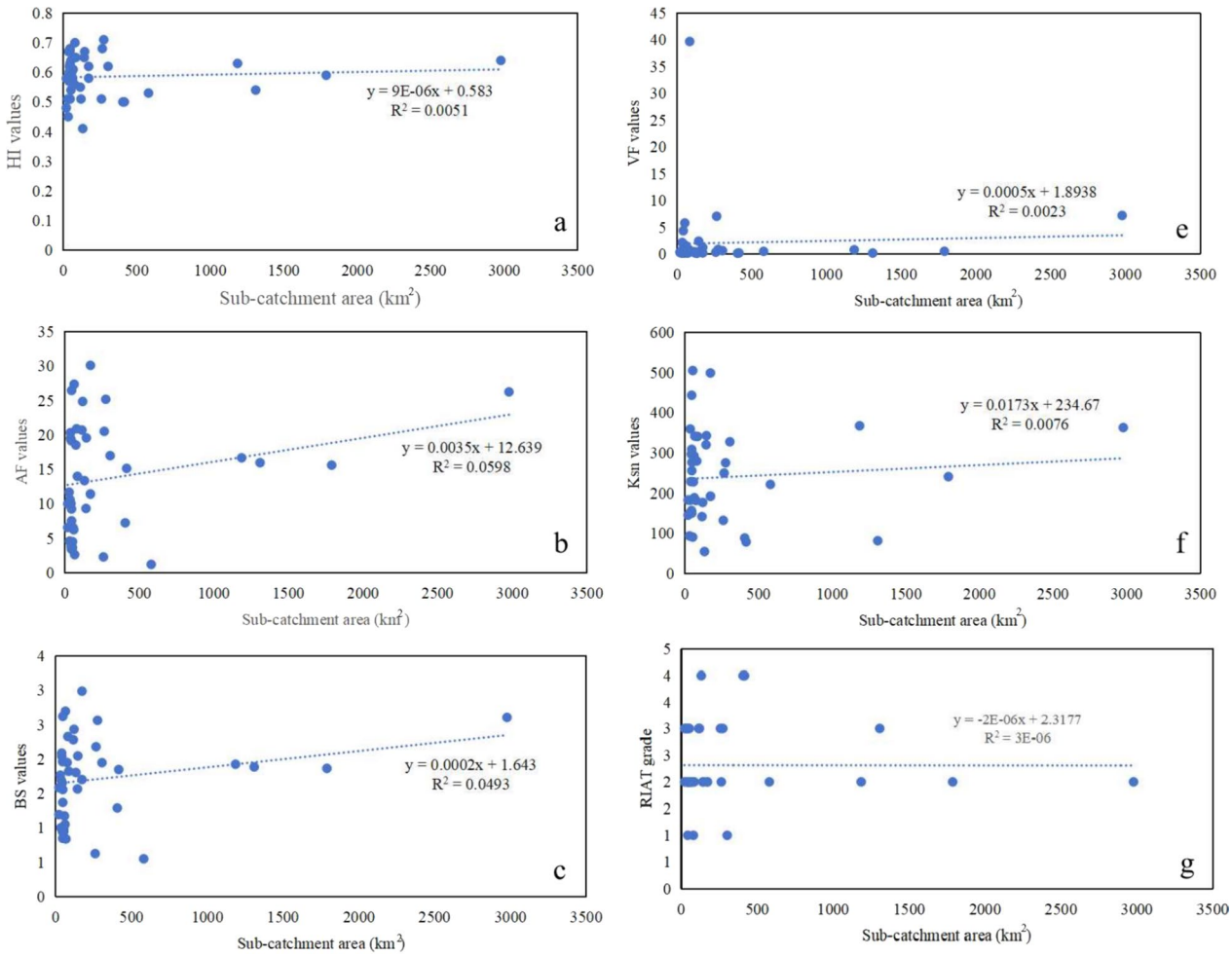

Fig. 15 The linear relationship between the geomorphic parameter values of each sub-catchment of SRC and the catchment area

intensity, field geological survey, and low-temperature thermochronology.

7 Conclusions

In this work, we used computer programs and data models such as GIS, numerical analysis tool, and DEM to extract various fluvial geomorphic parameters, and actively discussed the main controlling factors affecting the geomorphic evolution of the study area combining regional geological, glacier, precipitation and other data. We also graded the results of these geomorphic parameters and combined them with the geochronological data obtained from previous geochronological work in the study area to discuss the intensity of active tectonic activity in the region. Some positive conclusions we obtained.

Precipitation and glacier factors have little impact on the geomorphic evolution of the SRC, and some stream sections are controlled by lithology. However, geological tectonic activity and differential tectonic uplift are still the most important factors controlling the geomorphic evolution of the SRC. Because within the SRC, the distribution of active faults is consistent with the values of fluvial geomorphic parameters. That is, in areas with more active faults, the level of these parameter values is higher, which correspondingly shows stronger regional tectonic activity intensity.

Under the influence of differential tectonic uplift movement, the intensity of activity tectonic in the area is generally strong. The *VF* and *HI* indexes values in the catchment are high level. The streams of SRC are generally incised powerfully, therefore the valleys are relatively deep. Most of the streams are in transient state and the k_{sn} values are large, and the stream longitudinal profile is relatively steep, accompanied by the development of numerous knickpoints. From these parameter results, it can know that lithology only affects local

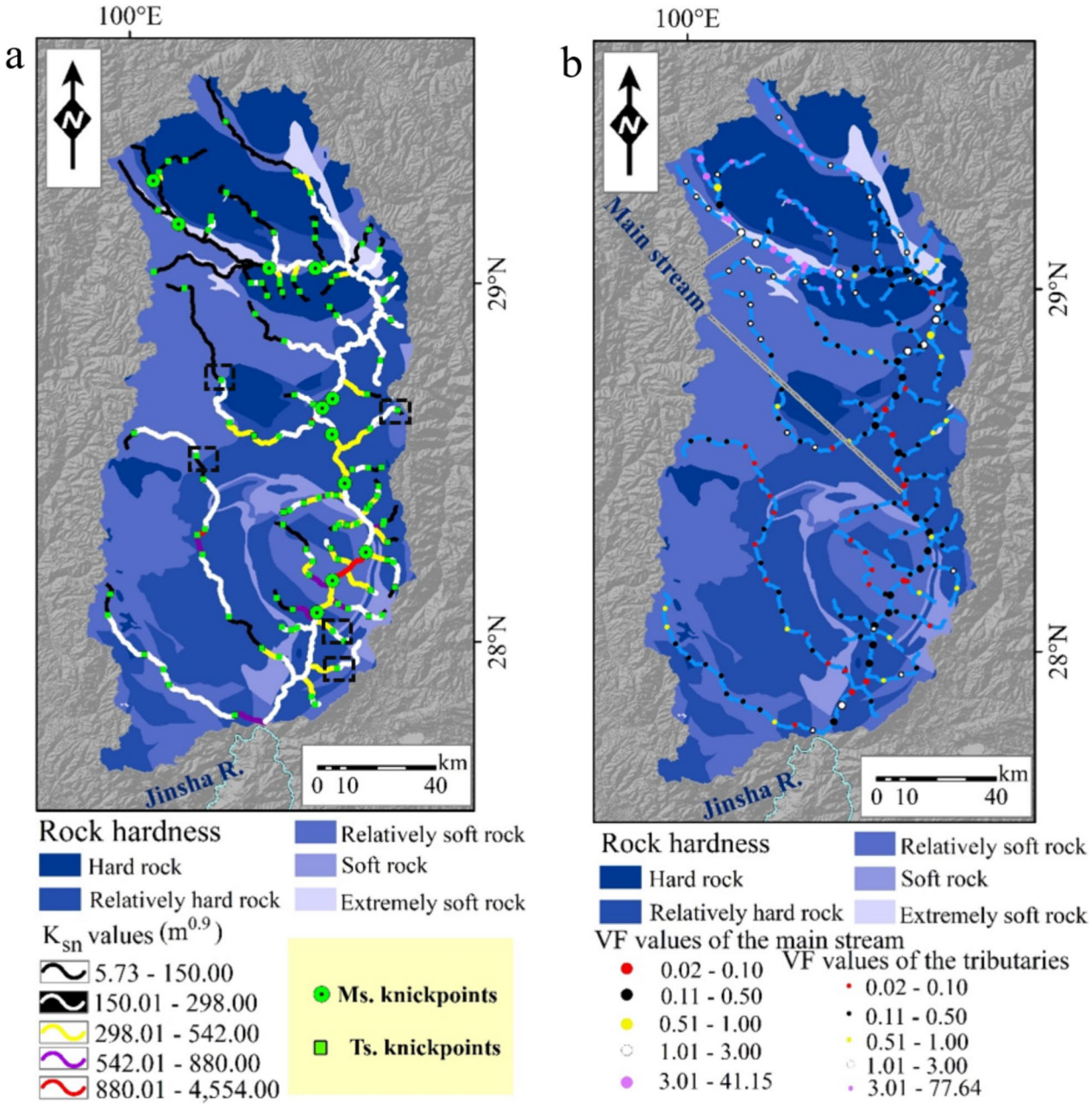

Fig. 16 The spatial distribution map of k_{sn} and *VF* values and the distribution map of rock erosion resistance of SRC. Note: the black dashed rectangular boxes exist in (**a**), which represent a positive correlation between the k_{sn} values of the river section and rock strength; **b** Overlay plot of *VF* value and rock strength

areas (or river sections). The intensity of activity tectonic in the midstream and downstream is strong, and the level of geomorphic parameters values are relatively high. The tectonic activity in the upstream is weak, and the *RIAT* are also small. The result of values of parameters indicates that the intensity of tectonic activity in the downstream is the greatest in the SRC. The results of geomorphic parameters extraction are also in good agreement with the regional seismic intensity, fieldwork and low-temperature thermochronology indicating that it is reasonable to use the fluvial geomorphic parameters to evaluate the crustal stability of the region, and the method of geomorphic parameters can well quantify the regional geomorphic evolution. Our

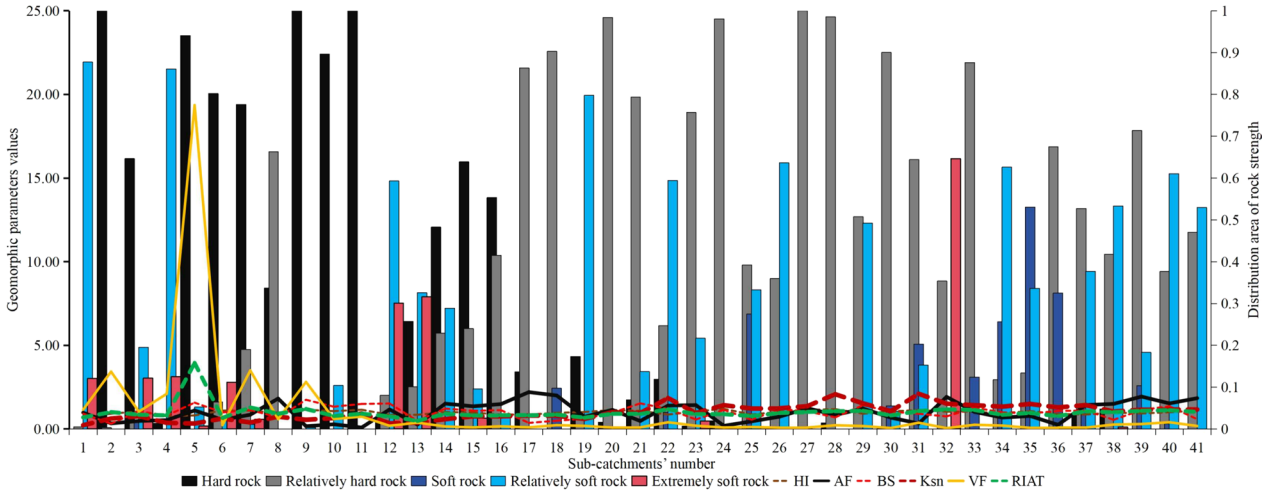

Fig. 17 The proportion of rock strength distribution area in each sub-catchments and the geomorphic parameters of each sub-catchment. Note that the values of geomorphic parameters have been dimensionless

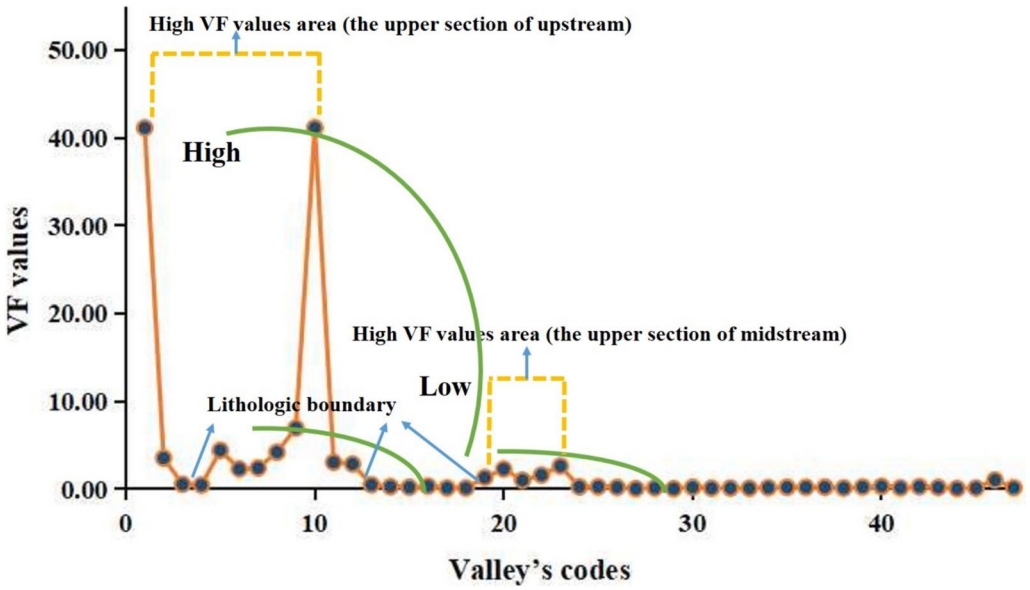

Fig. 18 Statistical diagram of 47 river valleys on the main stream of SRC

research indicates that the differences in tectonic activity intensity reflected by the fluvial geomorphology of SRC well respond to the differential uplift on the southeastern edge of the Tibetan Plateau. However, our work has only yielded a preliminary result. The interpretation of active faults, higher precision lithology data, and geochronology work are still insufficient, which may require further exploration.

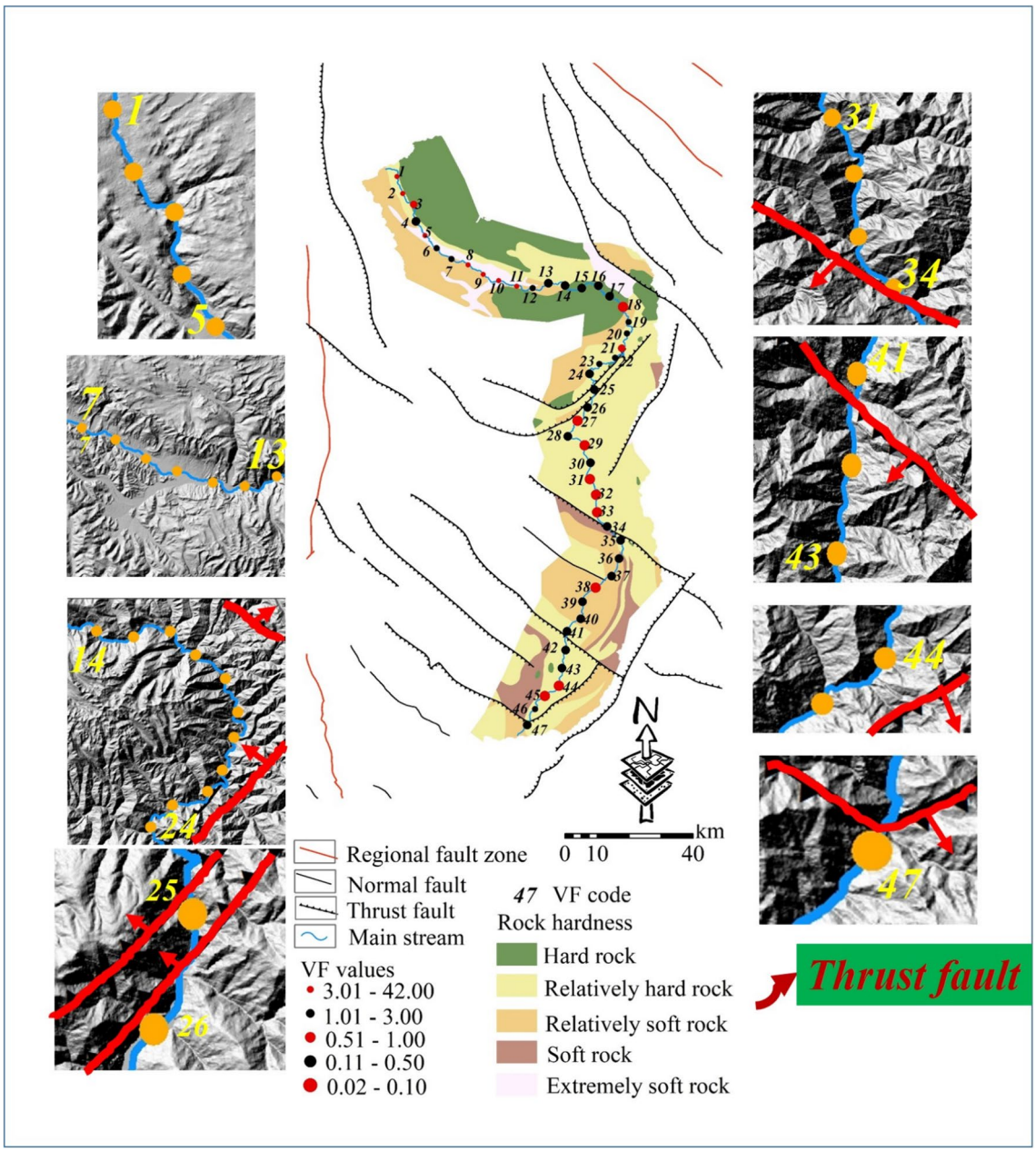

Fig. 19 The spatial distribution map of 47 river valleys in the main stream of SRC. The mountain shadow map of DEM is an enlarged figure of the local valley of DEM. The orange dots represent the calculated valleys

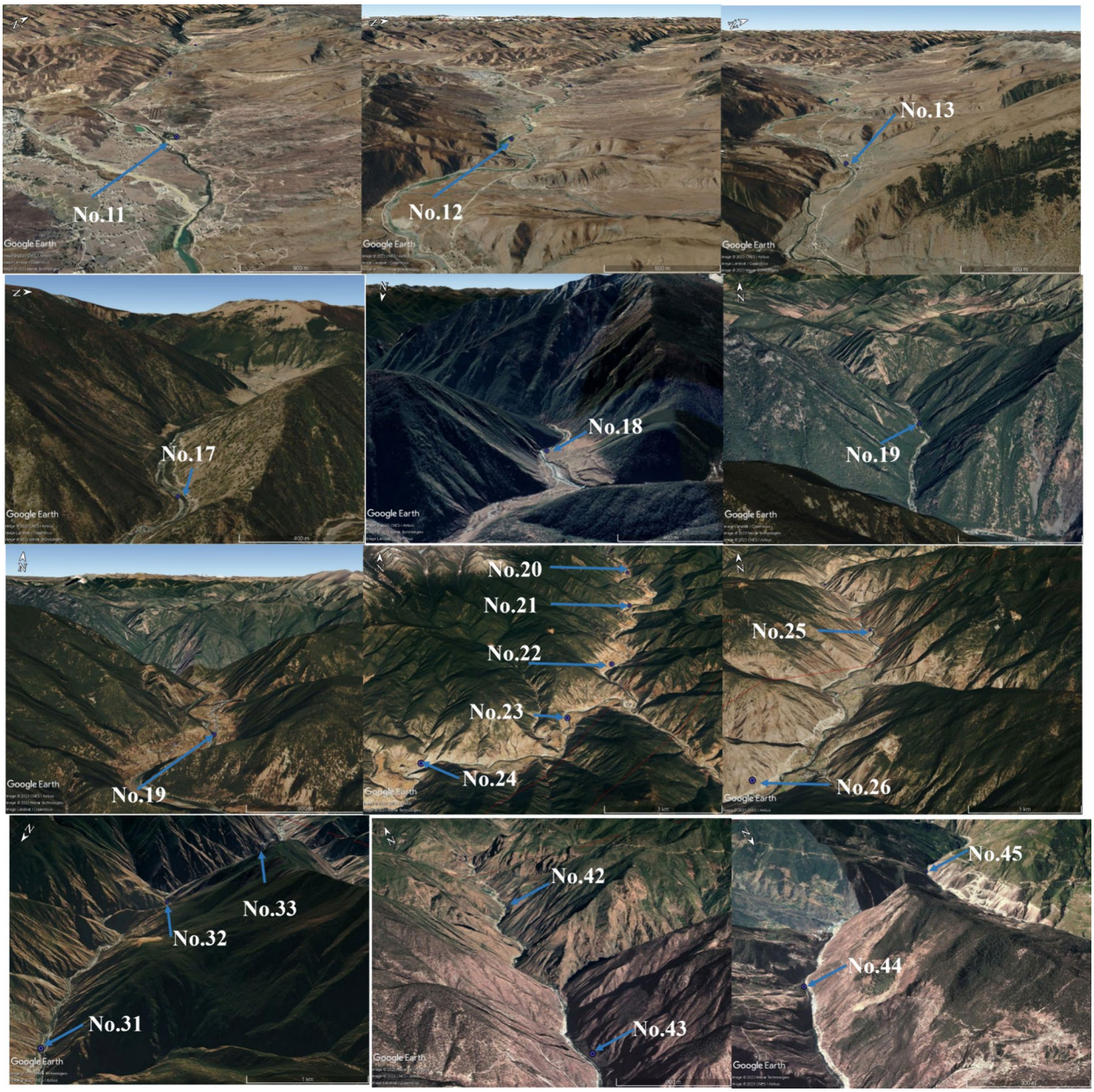

Fig. 20 The image of the valleys on the main stream of SRC from Google Earth Image. The valley shown in the figure are mainly the valleys in the lower part of the upstream and the upper part of the midstream. It can be clearly seen from the figure that these valleys are narrowing. The change from the 12th valley to the 13th valley are particularly significant; the valley in the middle and lower reaches can be clearly seen from the figure that are very narrow as a whole, basically deep V-shaped valleys, and the variation of *VF* value is not significant (Nos. 17–26). The valleys 31, 32, 33, 44 and 45 located on the side of the downfall wall of the thrust fault are the deepest valleys in the whole main stream, and the *VF* values are also very low

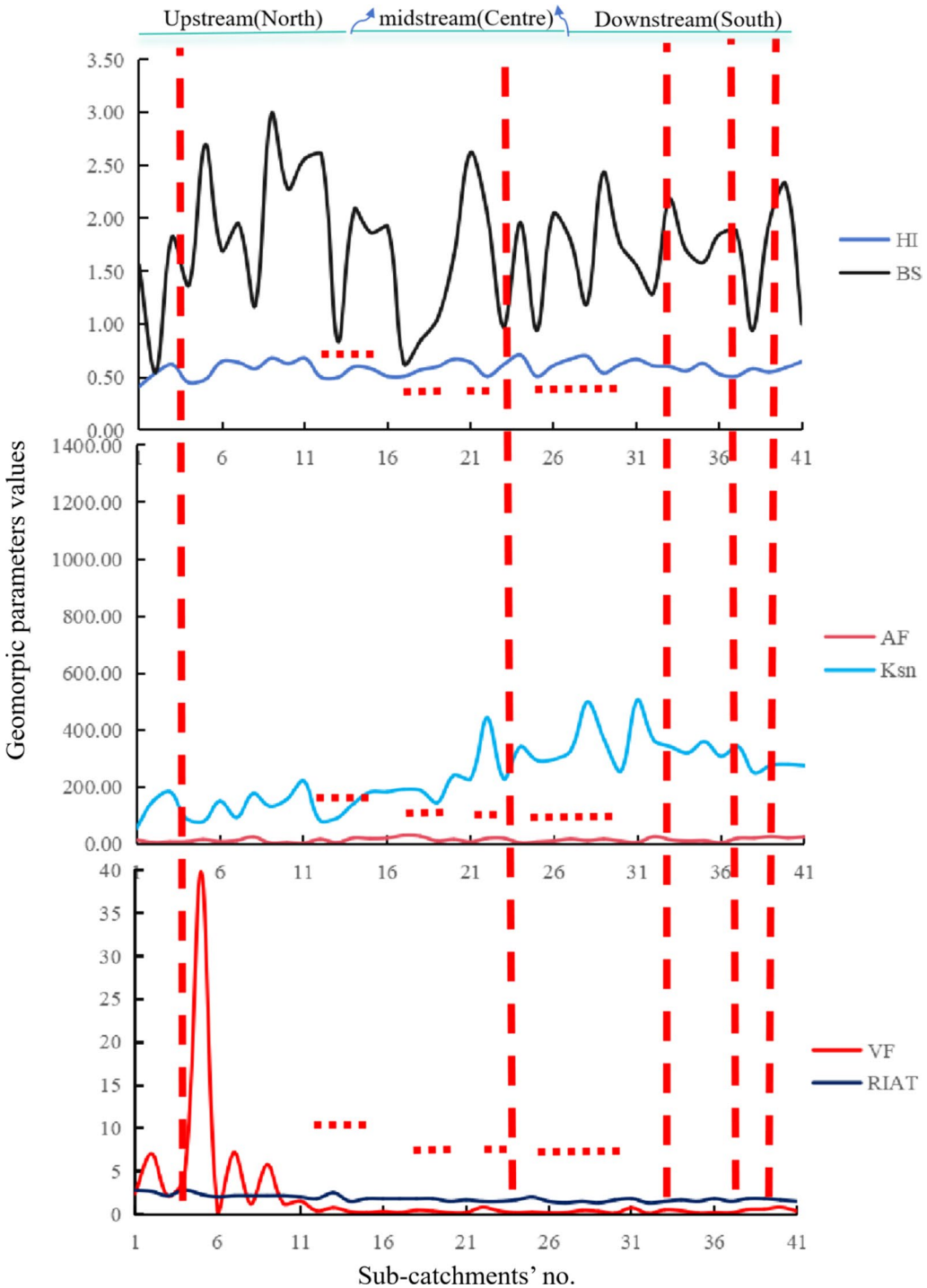

Fig. 21 The relationship between each parameter value and the spatial distribution of faults. The red dashed line in the figure represents the fault passing through the sub-catchments

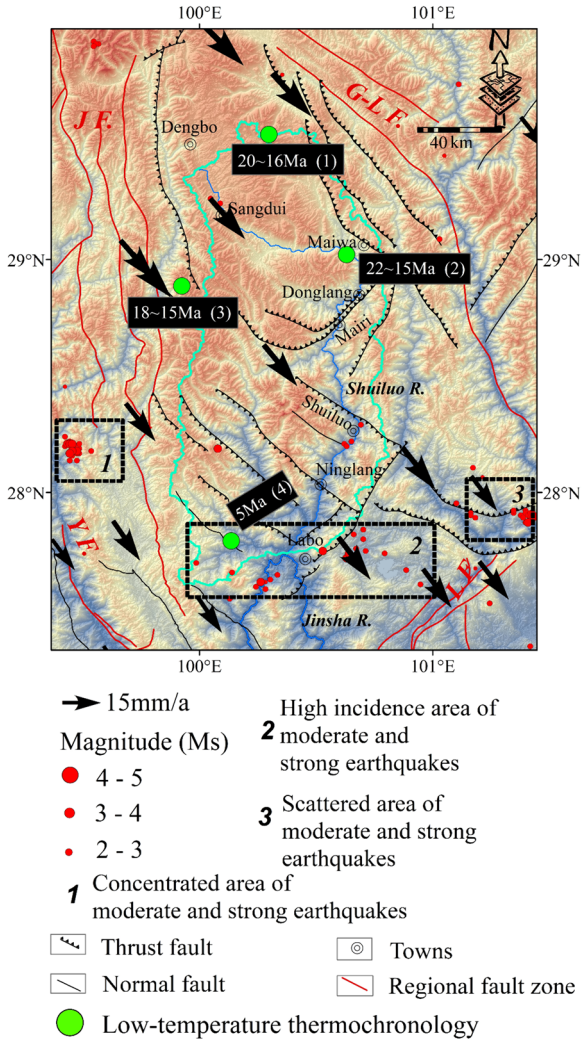

Fig. 22 The structural diagram and seismic distribution map of SRC are from China Earthquake Networks Center (https://news.ceic.ac.cn/index.html). Low-temperature thermochronology data are from: (1) Lai et al. (2007); (2) Tian et al. (2014); (3) Gourbet et al. (2019); (4) Zou et al. (2014). The black arrow represents the motion field captured by Global Navigation Satellite System (GNSS), which are from Wang and Shen (2019)

Acknowledgements
We sincerely thank the editor and two anonymous reviewers for their efforts in improving the quality of our manuscript.

Author contributions
YW is responsible for drafting and writing manuscripts, as well as extracting various data; LXX helped build the basic logical framework of our manuscript, provided higher resolution geological data, drone photos in field work, and he provided great assistance in revising our manuscript; LDN raised scientific issues and provided ideas, which played a role in supervising and reviewing the structure and data authenticity of the manuscript; WP provided guidance on some theoretical knowledge, such as the replacement of geomorphic evolution cycles and the significance of detrital zircon dating work; at the same time, we would like to thank all the authors for their assistance in field geological work.

Funding
This research was supported by the Guizhou Provincial Basic Research Program (Natural Science) (No. Yiban 436 2024 Qiankehe Jichu-ZK) and the Scientific Research Fund of Institute of Seismology and Institute of Crustal Dynamics, China Earthquake Administration (Grant No.IS 2018126278).

Availability of data and materials
The NASA DEM data are from https://www.earthdata.nasa.gov/esds/competitive-programs/measures/nasadem; the range of our study area is 99°26′22.02"E–101°31′52.50"E, 27°13′9.95 "N ~ 30°44′2.58"N; the geological data are from https://geocloud.cgs.gov.cn/, resolution is 1:500,000; the data of precipitation are from https://psl.noaa.gov/data/gridded/data.UDel_AirT_Precip.html; time range of the data is from 1991 to 2020; the data of Glacial lakes in the Qinghai Tibet Plateau and adjacent areas 1:2 million (2008) were obtained from http://www.ncdc.ac.cn/portal/; and the earthquake data are from China Earthquake Networks Center (https://news.ceic.ac.cn/index.html).

Declarations

Ethics approval and consent to participate statement
The research was carried out in accordance with a named standard.

Competing interests
The authors declare that they have no competing interests. And we promise to abide by the publication rules and agreements of the journal.

Received: 11 October 2023 Accepted: 3 June 2024
Published online: 12 June 2024

References

Alipoor R, Poorkermani M, Zare M, Hamdouni RE (2011) Active tectonic assessment around rudbarlorestan dam site, high zagros belt (SW of Iran). Geomorphology 128(1–2):1–14. https://doi.org/10.1016/j.geomorph.2010.10.014

Aier I, Luirei K, Bhakuni SS, Thong GT, Kothyari GC (2011) Geomorphic evolution of medziphema intermontane basin and quaternary deformation in the schuppen belt, Nagaland, NE India. Z Geomorphol 55(2):247–265. https://doi.org/10.1127/0372-8854/2011/0055-0048

Ahmad S, Alam A, Ahmad B, Afzal A, Bhat MI, Sultan BM, Farooq AH (2018) Tectono-geomorphic indices of the Erin basin, NE Kashmir valley, India. J Asian Earth Sci 151:16–30. https://doi.org/10.1016/j.jseaes.2017.10.013

Anand AK, Pradhan SP (2019) Assessment of active tectonics from geomorphic indices and morphometric parameters in part of Ganga basin. J Mt Sci-Engl 16(8):1943–1961. https://doi.org/10.1007/s11629-018-5172-2

Amine A, El Ouardi H, Zebari M, El Makrini H (2020) Active tectonics in the Moulay Idriss Massif (South Rifian Ridges, NW Morocco): New insights from geomorphic indices and drainage pattern analysis. J Afr Earth Sci 167:103833. https://doi.org/10.1016/j.jafrearsci.2020.103833

Ali U, Ali SA, Yousuf M, Rasool QA, Ahmad I (2021) Consideration of geomorphic indices in assessment of relative active tectonics in a part of seismogenic compressional kashmir basin. Arab J Geosci 14:1266. https://doi.org/10.1007/s12517-021-07523-3

Bull WB, Mcfadden LD (1977) Tectonic geomorphology north and south of the Garlock Fault, California. Synthetic Met. https://doi.org/10.1016/S0379-6779(00)01411-9

Burchfiel BC, Chen Z, Liu Y, Royden LH (1995) Tectonics of the Longmen Shan and adjacent regions. Int Geol Rev 37:661–735

Burbank DW, Leland J, Fielding E, Anderson RS, Brozovic N, Reid MR, Duncan C (1996) Bedrock incision, rock uplift and threshold hillslopes in the northwestern Himalayas. Nature 379(6565):505–510. https://doi.org/10.1038/379505a0

Bahrami S, Aghda S, Bahrami K, Rad MM, Poorhashemi S (2015) Effects of weathering and lithology on the quality of aggregates in the alluvial fans of northeast rivand, sabzevar, iran. Geomorphology 241:19–30. https://doi.org/10.1016/j.geomorph.2015.03.028

Buczek K, Górnik M (2020) Evaluation of tectonic activity using morphometric indices: case study of the tatra mts (western carpathians, poland). Environ Earth Sci 79:176. https://doi.org/10.1007/s12665-020-08912-9

Cannon PJ (1976) Generation of explicit parameters for a quantitative geomorphic study of the Mill Creek drainage basin. Oklahoma Geol Notes 1:3–16

Cox RT (1994) Analysis of drainage-basin symmetry as a rapid technique to identify area of possible Quaternary tilt-block tectonics: an example from Mississippi embayment. Geol Soc Am Bull 106(5):571–581. https://doi.org/10.1130/0016-7606(1994)106%3c0571:AODBSA%3e2.3.CO;2

Clark MK, Handy Royden L (2000) Topographic ooze: building the eastern margin of tibet by lower crustal flow. Geology 28(8):703–706. https://doi.org/10.1130/0091-7613(2000)028%3c0703:tobtem%3e2.3.co;2

Cyr AJ, Granger DE, Olivetti V, Molin P (2010) Quantifying rock uplift rates using channel steepness and cosmogenic nuclidedetermined erosion rates: examples from northern and southern Italy. Lithosphere 2:188–198. https://doi.org/10.1130/L96.1

Cyr AJ, Granger DE, Olivetti V, Molin P (2014) Disinguishing between tectonic and lithologic controls on bedrock channel longitudinal profiles using cosmogenic 10be erosion rates and channel steepness index. Geomorphology 209:27–38. https://doi.org/10.1016/j.geomorph.2013.12.010

Chang ZY, Sun WH, Wang J, Bai SB, Zhang ZG (2015) Application of DEM in the morphological analysis of tectonic geomorphology: status and prospect. J Nanjing Norm Univ Nat Sci Ed 38(4):139–136. https://doi.org/10.3969/j.issn.1001-4616.2015.04.023(inChinesewithEnglishabstract)

Chen G, Xu XW, Wen XZ, Chen YG (2016) Late quaternary slip-rates and slip partitioning on the Southeastern Xianshuihe fault system. Eastern Tibetan Plateau Acta Geol Sin-Engl 90(2):537–554. https://doi.org/10.1111/1755-6724.12689

Chen L, Capitanio FA, Liu L, Gerya TV (2017) Crustal rheology controls on the Tibetan plateau formation during India-Asia convergence. Nat Commun 8:15992. https://doi.org/10.1038/ncomms15992

Chen M, Hu XF, Wang W (2018) The cause of high-altitude knickpoints on river longitudinal profiles along the Zoulang Nan Shan. Acta Geol Sin-Engl 73(9):1702–1713. https://doi.org/10.11821/dlxb201809007

Chang YQ, Chen LC, Zhang Q (2019) Study on tectonic geomorphology and fault activity characteristics of Jinshajiang Fault zone. Recent Dev Word Seismol 8:142–143. https://doi.org/10.3969/j.issn.0253-4975.2019.08.114

Chen Y, Zhang G, Lu R, Luo T, Li Y, Yu W (2020) Formation and evolution of Xianshuihe Fault Belt in the eastern margin of the Tibetan Plateau: constraints from structural deformation and geochronology. Geol J 55(12):7953–7976. https://doi.org/10.1002/gj.3908

Chen B, Yu Z, Li L, Zheng R, Wu C (2023) Surface deformation and damage of 2022 (M6.8) Luding earthquake in China and its tectonic implications. Open Geosci 15(1):20220490. https://doi.org/10.1515/geo-2022-0490

Duan JZ, Tan XH (2000) The nature and feature of Cenozoic main strike-slip fault in the Three-River area of west Yunnan. Yunnan Geol 19:8–23 (**(in Chinese with English abstract)**)

Ding R, Ren JJ, Zhang SM, Lv YW, Liu HY (2018) Late quaternary paleoearthquakes on the middle segment of the Lijiang-Xiaojiang Fault. Southeastern Tibet. Seismol Geol 40(3):622–640. https://doi.org/10.3969/j.issn.2053-4967.2018.03.009. (**(in Chinese with English abstract)**)

Ding L, Kapp P, Cai F, Garzione CN, Xiong Z, Wang H, Wang C (2022) Timing and mechanisms of Tibetan Plateau uplift. Nat Rev Earth Environ 3(10):652–667. https://doi.org/10.1038/s43017-022-00318-4

England P (1997) Active deformation of Asia: from kinematics to dynamics. Science 278(5338):647–650. https://doi.org/10.1126/science.278.5338.64

Flint JJ (1974) Stream gradient as a function of order, magnitude, and discharge. Water Resou Res 10(5):969–973. https://doi.org/10.1029/wr010i005p00969

Fan YL, Pan BT, Hu ZB, Ren DY, Chen QW, Liu FL, Li ZM (2018) An Analysis of tectonic geomorphologic characteristics of the Beipanjiang Basin in the Yunnan-Guizhou Plateau. Adv Earth Sci 33(7):751–761. https://doi.org/10.11867/j.issn.1001-8166.2018.07.0751. (**(in Chinese with English abstract)**)

Gao XD, Xie H, Yuan DY, Su Q, Shao YX (2019) Longitudinal profile and their tectonic significance of the Shiyanghe River Basin in the Eastern Qilianshan Mountain. Seismol Geol 41(2):320–340. https://doi.org/10.3969/j.issn.0253-4967.2019.02.005. (**(in Chinese with English abstract)**)

Gourbet L, Yang R, Fellin MG, Paquette JL, Willett SD, Gong J, Maden C (2019) Evolution of the Yangtze river network, southeastern Tibet: Insights from thermochronology and sedimentology. Lithosphere-Us 12:3–18. https://doi.org/10.1130/l1104.1

Howard AD, Kerby G (1983) Channel changes in badlands. Geol Soc Am Bull 94:739–752. https://doi.org/10.1130/0016-7606(1983)94%3c739:CCIB%3e2.0.CO;2

Hare PW, Gardner TW (1985) Geomorphic indicators of vertical neotectonism along converging plate margins, Nicoya Peninsula, Costa Rica. Paper presented at tectonic geomorphology-proceeding of the 15th annual Binghamton geomorphology symposium, Boston

Hao ZW, Yao DS, X WJ, Hu JC, Wang ZS (1990) Regional geology of Sichuan Provence. Geological publishing house, Beijing (in Chinese)

Howard AD, Dietrich WE, Seidl MA (1994) Modeling fluvial erosion on regional to continental scales. J Geophys Res-Sol Ea 99(B7):13971–13986. https://doi.org/10.1029/94jb00744

Hamdouni RE, Irigaray C, Fernández T, Chacón J, Keller EA (2008) Assessment of relative active tectonics, southwest border of the sierra nevada (Southern Spain). Geomorphology 96(1–2):150–173. https://doi.org/10.1016/j.geomorph.2007.08.004

He HL, Ran HL, Yasutaka I (2010) Uniform strike-slip rate along the Xianshuihe-Xiaojiang fault system and its implications for active tectonics in southeastern tibet. Acta Geol Sin-Engl 80(3):376–386. https://doi.org/10.1111/j.1755-6724.2006.tb00255.x

He ZY, Zhong LL, Cao K, Su WB, Glorie S, Zhong KH, Sun C, DeGrave J (2023) New constraints on the late oligocene-miocene thermo-tectonic evolution of the southeastern tibetan plateau from low-temperature thermochronology. Tectonics 42(8):e2023TC007881. https://doi.org/10.1029/2023TC007881

Huang Y, Guo Y (2023) Risk assessment of rain-induced debris flow in the lower reaches of Yajiang River based on GIS and CF coupling modes. Open Geosci 15(1):20220472. https://doi.org/10.1515/geo-2022-0472

Jackson WT, Robinson DM, Weisloge AL, Jian X (2020) Cenozoic reactivation along the late triassic ganzi-litang suture, eastern tibetan plateau. Geosci Front 11(3):1069–1080. https://doi.org/10.1016/j.gsf.2019.11.001

Ji L, Zhang W, Liu C, Zhu L, Xu J, Xu X (2020) Characterizing interseismic deformation of the Xianshuihe fault, eastern Tibetan Plateau, using Sentinel-1 SAR images. Adv Spa Res 66(2):378–394. https://doi.org/10.1016/j.asr.2020.03.043

Kirby E, Whipple KX, Tang W, Chen Z (2003) Distribution of active rock uplift along the eastern margin of the Tibetan Plateau: inferences from bedrock channel longitudinal profiles. J Geophy Res-Solid Earth. https://doi.org/10.1029/2001jb000861

Kirby E, Whipple KX (2012) Expression of active tectonics in erosional landscapes. J Struct Geol 44:54–75

Kong P, Zheng Y, Caffee MW (2012) Provenance and time constraints on the formation of the first bend of the Yangtze River. Geochem Geophy Geosyst 13:6. https://doi.org/10.1029/2012GC004140

Lai Q, Ding L, Wang H, Yue Y, Cai F (2007) Constraining the stepwise migration of the eastern Tibetan Plateau margin by apatite fission track thermochronology. Sci China Ser D 50:172–183. https://doi.org/10.1007/s11430-007-2048-7

Lahiri SK, Sinha R (2014) Morphotectonic evolution of the majuli island in the brahmaputra valley of assam, india inferred from geomorphic and geophysical analysis. Geomorphology 227:101–111. https://doi.org/10.1016/j.geomorph.2014.04.032

Li S, Deng C, Dong W, Sun L, Liu S, Qin H, Zhu R (2015) Magnetostratigraphy of the Xiaolongtan formation bearing Lufengpithecus keiyuanensis in Yunnan, southwestern China: Constraint on the initiation time of the southern segment of the Xianshuihe-Xiaojiang fault. Tectonophysics 655:213–226. https://doi.org/10.1016/j.tecto.2015.06.002

Li C, Xu W, Wu J, Gao M (2016) Using new models to assess probabilistic seismic hazard of the North-South Seismic Zone in China. Nat Hazards 82:659–681. https://doi.org/10.1007/s11069-016-2212-5

Li X, Hergert T, Henk A, Zeng Z (2021) Contemporary kinematics in the eastern Tibetan Plateau: Insights from 3D geomechanical modeling. Tectonophysics 819:229109. https://doi.org/10.1016/j.tecto.2021.229109

Luo Q, Schoenbohm L, Rimando J, Li Y, Li C, Xiong J (2023) Morphometric analysis of the North Liuleng Shan Fault in the northern Shanxi Graben System, China: insights into active deformation pattern and fault

evolution. Geomorphology 440:108862. https://doi.org/10.1016/j.geomorph.2023.108862
Molnar P, Tapponnier P (1975) Cenozoic tectonics of Asia: effects of a continental collision. Science 189(4201):419–426. https://doi.org/10.2307/1740465
Ma H, Zhang H, Li M, Wu S, Wang P, Wang Q, Zhao J, Ma Z (2023a) Characteristics of the present crustal deformation in the Tibetan Plateau and its relationship with strong earthquakes. Open Geosci 15(1):20220387. https://doi.org/10.1515/geo-2022-0387
Ma Z, Peng T, Feng Z, Li X, Song C, Wang Q, Tian W, Zhao X (2023b) Tectonic and climate controls on river terrace formation on the northeastern Tibetan Plateau: evidence from a terrace record of the Huangshui River. Quatern Int 656:16–25. https://doi.org/10.1016/j.quaint.2022.11.004
Nie F, Fan WY, Liu SS (2015) Structural characteristics of the suoluogou gold deposit in Muli County, West Sichuan Province. Acta Geol Sin-Engl 89(15):1773–1774. https://doi.org/10.1111/1755-6724.12583
Pérez-Peña JV, Azor AA, Zañón JM, Keller EA (2010) Active tectonics in the Sierra Nevada (Betic Cordillera, SE Spain): insights from geomorphic indexes and drainage pattern analysis. Geomorphology 119(1–2):74–87. https://doi.org/10.1016/j.geomorph.2010.02.020
Partabian A, Nourbakhsh A, Ameri S (2016) GIS-based evaluation of geomorphic response to tectonic activity in Makran Mountain Range, SE of Iran. Geosci J 20(6):921–934. https://doi.org/10.1007/s12303-016-0106-xFaghih
Reid A, Wilson CJ, Shun L, Pearson N, Belousova E (2007) Mesozoic plutons of the Yidun Arc, SW China: U/Pb geochronology and Hf isotopic signature. Ore Geol Rev 31(1–4):88–106. https://doi.org/10.1007/s12145-013-0121-7
Strahler AH (1952) Hypsometric (area-altitude) analysis of erosional topography. Geol Soc Am Bull 63(11):1117–1142. https://doi.org/10.1130/0016-7606(1952)63[1117:haaoet]2.0.co;2
Sklar L, Dietrich WE. Tinkler KJ, Wohl EE (eds) (1998) River longitudinal profiles and bedrock incision models: stream power and the influence of sediment supply. Geophys Monogr-Am Geophy Union 107:237–260
Snyder NP, Whipple KX, Tucker GE, Merritts DJ (2000) Landscape response to tectonic forcing: digital elevation model analysis of stream profiles in the Mendocino triple junction region, northern California. Geol Soc Am Bull 112(8):1250–1263. https://doi.org/10.1130/0016-7606(2000)112%3c1250:lrttfd%3e2.3.co;2
Su Q, Yuan D, Xie H (2016) Geomorphic features of the Heihe RiverDrainage Basin in Western Qilianshan-Hexi Corridor and its tectonic implications. Seismol Geol 38(3):560–581. https://doi.org/10.3969/j.issn.0253-4967.2016.03.005(inChinesewithEnglishabstract)
Sun J, Ding Z, Xiao W, Windley BF (2022) Coupling between uplift of the Central Asian Orogenic Belt-NE Tibetan Plateau and accumulation of aeolian Red Clay in the inner Asia began at~7 Ma. Earth-Sci Rev 226:103919. https://doi.org/10.1016/j.earscirev.2022.103919
Shi Y, Gao Y, Zhang H, Zhang Z, Li G (2023) Crustal azimuthal anisotropy in the lateral collision zone of the SE margin of the Tibetan Plateau and its tectonic implications. Geophys J Int 234(1):1–11. https://doi.org/10.1093/gji/ggad059
Sun Y, Li H, Fan T, Li B (2023) Effect of rheological heterogeneities on the lithospheric deformation of the Tibetan Plateau and neighbouring regions. Front Earth Sc-Swith 11:1153744. https://doi.org/10.1093/gji/ggad059
Tapponnier P, Molnar P (1977) Active faulting and tectonics in China. J Geophys Res 82(20):2905–2930. https://doi.org/10.1029/jb082i020p02905
Tapponnier P (2001) Oblique stepwise rise and growth of the Tibet Plateau. Science 294(5547):1671–1677. https://doi.org/10.1126/science.105978
Tang RC, Han WB (1993) Active faults and earthquakes and in Sichuan Province. Seismological Press, Beijing (**(in Chinese)**)
Tang GA, Na JM, Chen WM (2017) Progress of digital terrain analysis on regional geomorphology in China. Acta Geoda Cartogra Sin 46(10):1570–1591. https://doi.org/10.11947/j.AGCS.2017.20170388. (**(in Chinese with English abstract)**)
Tian Y, Kohn BP, Gleadow AJW, Hu S (2014) A thermochronological perspective on the morphotectonic evolution of the southeastern Tibetan Plateau. J Geophys Res-Solid Earth 119:676–698. https://doi.org/10.1002/2013JB010429
Tian J, Pang Z, Liao D, Zhou X (2021) Fluid geochemistry and its implications on the role of deep faults in the genesis of high temperature systems in the eastern edge of the Qinghai Tibet Plateau. Appl Geochem 131:105036. https://doi.org/10.1016/j.apgeochem.2021.105036
Tian H, Chen H, Cheng X, Wu L, Lin X, Gao S, Li F, Xu X, Yin Q (2023) Limited northward expansion of the Tibetan Plateau in the Late Cenozoic: insights from the cherchen fault in the Southeastern Tarim Basin. Tectonics 42(7):e2022TC007694. https://doi.org/10.1029/2022TC007694
Tan S, Tian X, Zeng X, Nie F, Qu C, Yu C (2023) Crustal structure beneath the northern part of the southeastern Tibetan Plateau revealed by a seismic dense nodal array. J Asian Earth Sci 258:105593. https://doi.org/10.1016/j.jseaes.2023.105593
Williams PW (1987) Geomorphic inheritance and the development of tower karst. Earth Surf Proc Lan 12(5):453–465. https://doi.org/10.1002/esp.3290120503
Whipple KX, Tucker GE (1999) Dynamics of the stream power river incision model: implications for height limits of mountain ranges, landscape response timescales, and research needs. J Geophy Res Solid Earth 104(B8):17661–17674. https://doi.org/10.1029/1999JB900120
Whipple KX (2004) Bedrock rivers and the geomorphology of active orogens. Annu Rev Earth Plant Sci 32:151–185. https://doi.org/10.1146/annurev.earth.32.101802
Wobus CW, Whipple KX, Kirby E (2006) Tectonics from topography: procedure, promise, and pitfalls. Geol Soc Am Bull 398:55–74
Wang S, Fan C, Wang G, Wang E (2008) Late Cenozoic deformation along the northwestern continuation of the Xianshuihe fault system, Eastern Tibetan Plateau. Geol Soc Am Bull 120(3–4):312–327. https://doi.org/10.1130/b25833.1
Wang E, Meng K, Su Z, Meng Q, Chu JJ, Chen Z, Liang X (2014) Block rotation: tectonic response of the Sichuan basin to the southeastward growth of the Tibetan Plateau along the Xianshuihe-Xiaojiang fault. Tectonics 33(5):686–718. https://doi.org/10.1002/2013tc003337
Wang M, Shen ZK (2020) Present-day crustal deformation of continental China derived from GPS and its tectonic implications. J Geophys Res-Solid Earth 125(2):e2019JB018774. https://doi.org/10.1029/2019JB018774
Wang YZ, Zheng DW, Zhang HP, Yu JX, Pang JZ (2020) Hao YQ (2020) Channel profile response to abrupt increases in mountain uplift rates: Implications for Late Miocene to Pliocene acceleration of intracontinental extension in the Northern Qinling Range-Weihe Graben, Central China. Lithosphere 1:7866972. https://doi.org/10.2113/2020/7866972
Wang Y, Liu C, Zheng D, Zhang H, Yu J, Pang J, Li C, Hao Y (2021) Multistage exhumation in the catchment of the Anninghe River in the SE Tibetan Plateau: Insights from both detrital thermochronology and topographic analysis. Geophy Resh Lett 48(11):e2021GL092587. https://doi.org/10.1029/2021GL092587
Wang Y, Li C, Hao Y, Zheng D, Zhang H, Yu J, Pang J (2022) Multi-stage growth in the north margin of the Qinling Orogen, Central China, Revealed by both low-temperature thermochronology and River Profile Inversion. Tectonics 41(4):e2021TC007029. https://doi.org/10.1029/2021TC007029
Wu C, Sun X, Li G, Huang LQ, Jiao HJ, Li ZW, Jian X, Mason CC, Juan Pedro Rodríguez-López, JP (2023) Cretaceous mountain building processes triggered the aridification and drainage evolution in east Asia. Geol Soc Am Bull 136(5–6):1863–1877. https://doi.org/10.1130/B36763.1
Wu X, Guo Z, Li S, Yu Y, Bai Q, Chen YJ (2023) Seismic azimuthal anisotropy of northeastern Tibetan Plateau from ambient noise double beamforming tomography: Implication for crustal deformation. J Geophy Res-Solid Earth e2022JB026109. https://doi.org/10.1029/2022JB026109
Xu XW, Han ZJ, Yang XP, Zhang SM, Yu GH, Zhou BG, L F, Ma BQ, Chen GH, Rang YK (2016). Seismoteconic map in China and its adjacent region. Seismological Press, Beijing (in Chinese)
Xiong L, Tang G, Yang X, Li F (2021) Geomorphology-oriented digital terrain analysis: progress and perspectives. J Geogr Sci 31(3):456–476. https://doi.org/10.1007/s11442-021-1853-9
Yan B, Lin A (2017) Holocene activity and paleoseismicity of the Selaha Fault, southeastern segment of the strike-slip Xianshuihe Fault Zone, Tibetan Plateau. Tectonophysics 694:302–318. https://doi.org/10.1016/j.tecto.2016.11.014
Yin L, Luo G (2021) Fault interaction and active crustal extrusion in the southeastern Tibetan Plateau: insights from geodynamic modeling. J Asian Earth Sci 218:104866. https://doi.org/10.1016/j.jseaes.2021.104866
Yu L, Dong Y, Zhou W, Zhang D, Wang D, Yu H, Ren Y, Li J (2022) Evaluation of the Rock Uplift Pattern in the Central Yunnan Subblock, SE

Tibetan Plateau: Based on the Bedrock Channel Profile. Front Earth Sci 10:821367. https://doi.org/10.3389/feart.2022.821367
Zhou DQ, Liu XM, Jiang LJ, Liu CR (2005) Step-like landforms and uplift of Guizhou Plateau. Earth Environ 33:79–84
Zou B, Wang G, Deng J (2014) Evidence for apatite fission track of Pliocene rapid uplift of Zhongdian region on southeastern margin of Tibetan Plateau, China. J Chengdu Uni Technol 41:227–236. https://doi.org/10.3969/j.issn.1671-9727.2014.02.12(inChinesewithEnglishabstract)
Zhang J, Li WY, Tang XC, Tian J, Wang YC, Guo Q, Pang ZH (2017) Geothermal data analysis at the high-temperature hydrothermal area in Western Sichuan. Sci China Earth Sci 60:1507–1521. https://doi.org/10.1007/s11430-016-9053-2
Zhang D, Cao K, Yuan X, Wang G, Van DBP (2022) Late oligocene-early miocene origin of the first bend of the Yangtze River explained by thrusting-induced river reorganization. Geomorphology 411:108303. https://doi.org/10.1016/j.geomorph.2022.108303
Zhou Z, Yan D, Qiu L, Kong R, Song H, Xiao D, Lin X, Du C, Kong F (2023a) Multi-phase non-coaxial orogenic growth: propagation of the Longmen Shan Thrust Belt on the Eastern Margin of the Tibetan Plateau. Tectonics 42(9):e2023TC007814. https://doi.org/10.1029/2023TC007814
Zhou H, Liu S, Yang W, Yang D, Xu X, Li M, Wang W, Yang S (2023b) Deformation of the NE Tibetan plateau revealed by velocity and azimuthal anisotropy structures. Tectonophysics 856:229846. https://doi.org/10.1016/j.tecto.2023.229846

Publisher's Note